Reply to Comments from Reviewer #2

2   We appreciate the constructive and thoughtful comments from the reviewers which have helped

3   us improve the manuscript. We have carefully revised our manuscript following the reviewer's

4   comments. A point-to-point response is given below. The reviewers' comments are in black and our

5   replies are in blue.

6

7   **To reviewer**

8   *Comment 1:*

9   The authors report flux measurements of total gaseous mercury (TGM) on 5 plots in subtropical

10   forest and 5 plots in temperate forest in four seasons. They use the dynamic flow chamber (DFC)

11   method and describe the flux dependence on ambient TGM concentrations, solar radiation, and

12   temperature. The diurnal variations in different seasons are described.

13   The measurements are valuable but the authors stretch their interpretation by taking the

14   measured fluxes as being representative for the whole investigated ecosystems. DFC measurements

15   are well suited to study the flux mechanism, i.e. flux dependence on temperature, soil moisture,

16   ambient TGM concentration, solar radiation, soil temperature, substrate concentrations, etc. But

17   they are unsuitable for determination of the representative fluxes for a given ecosystem because a)

18   only a small area is being measured (20 x 30 cm here) and b) covering of the soil by DFC changes

19   its status (e.g. by heating the soil or vegetation by glasshouse effect). In other words: really

20   representative fluxes have to be measured by micrometeorological methods, DFC methods can

21   provide only empirical relationships for extrapolating them to the whole ecosystems. The problem

22   with this paper is that the authors try to estimate ecosystem fluxes as if their measurements were

23   representative for them, despite being aware of the problems in DFC measurements (mentioned in

24   meagre 3-4 lines).

25   I recommend the publication of the paper provided that the authors stick with the mechanistical

26   interpretation of their results and avoid the temptation of extrapolations to the whole ecosystems

27   (made e.g. in "Conclusions and study implications)". This would need some changes in the text.

28   The authors also discuss the observed correlations and relations predominantly in physicochemical

29   terms. By this they neglect the soil microbiology – this also needs to be rectified.

30   Response: We thank the reviewer for providing constructive and thoughtful comments on our

manuscript. We agree with the concern that there are some limitations of the use of DFCs to estimate ecosystem fluxes of Hg. We have deleted statements about estimates of whole ecosystem Hg fluxes in the revised paper, especially in the sections in the Abstract and Conclusions and study implications. This version of the paper now focuses on the mechanism of soil-air Hg exchange fluxes under different land cover conditions and discusses effects of temperature, incident solar radiation and precipitation on soil Hg exchange and implications of climate change induced transition of forest stands on Hg emissions. Additionally, we have also added discussion about the role of soil microbial transformations on TGM emissions as detailed in the comments below.

Comment 2:

Line 50: "..long longevity*: : :* is able to undergo over long distances.."?

Response: The sentence has revised in 54-56:

"Hg(0) is relatively inert and has a long atmospheric lifetime of 0.5–1 year, which allows for long range transport (Kamp et al., 2018;Slemr et al., 2018;St Louis et al., 2019).."

Comment 3:

Line 59: Not all fires are "natural".

Response: The text has been changed to "Although many studies have focused on primary anthropogenic Hg emissions, releases from natural source materials is also an important pathway but with greater uncertainty and variability, including emissions from natural reservoirs (e.g. volcanic activity, geothermal sources, weathering of Hg from soil minerals) and re-emissions of previous deposited Hg." in line 63-66.

Comment 4:

Lines 147-149: "semi-cylindical" and "20 x 30 cm" – how does it fit together? "Six inlet holes" where?

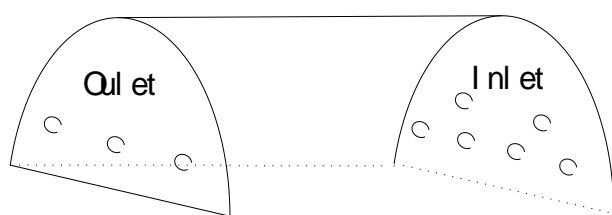Response: We have added the schematic drawing of the flux chamber in the Fig. S1.

Fig. S1. Schematic diagram of the dynamic flux chamber used in this study.

Comment 5:

Lines 147-153: How was the chamber installed on the soil: was it partly buried into the soil to seal the chamber-soil gap, if so to which depth? Are you sure that you do not suck ambient air through the soil or through the gap between the chamber and the soil, at least partly, instead of sucking air through the inlet holes? The resistance of the soil with respect to air flow can be surprisingly small, it may be smaller than the resistance of the inlet holes, resulting in sucking of air through the soil. If that happens, the measured fluxes are not what was intended to be measured. Eckley et al. (2010) do not mention this problem. If I understand the text properly then the chambers were permanently (during the measurement period) on the soil. If so, then the plot under measurement would e.g. not receive any precipitation? In other words: the measurements would not be representative for uncovered soil. Please specify.

Response: The chamber was not buried into the soil and placed on the top of the forest floor. To seal the chamber-soil gap, local fine soil was placed outside of the chamber bottom. We believe that the resistance of the fine soil (forest soil is relatively moisture) would be much higher than that of six inlets (1 cm in diameter) on the chambers. The chamber was not positioned in a fixed (during the measurement period) on the soil. Rather we moved the chambers to a new position as least every week when there was no rain and moved it to new position after days in which it rained. Therefore, the flux measurements are better able represent conditions under different weather. We have revised the text to clarify these approaches in lines 162-163 and 167-190:

"Local fine grained soil was placed outside the chamber to seal any gap between the base of the chamber and the soil."

"The DFC chambers in all plots were moved every week to mitigate against changes in soil moisture due the covering of soil by the chambers. If a precipitation event occurred, the chambers were also moved to new positions during the sampling period (morning or evening) to be

85   representative of soil conditions receiving ambient precipitation."

86

87   ***Comment 6:***

88   Gold cartridges: what type? Those of Tekran or other? Please specify.

89   Response: We made the gold cartridges in the laboratory and this is described in the revised text on

90   line 166-169:

91   "All the gold cartridges were constructed with gold silk (< 0.5 mm diameter). The strands of

92   gold silk were rolled together in a small coil and about 15 coils were used to fill a quartz cartridge

93   with about 2 g of gold. The accuracy of all traps were evaluated (see section 2.4) and non-

94   conforming cartridges were discarded."

95

96   ***Comment 7:***

97   Lines 176-178: In these few lines the authors mention the problems with fluxes measured by

98   DFC and, essentially, salvage themselves using Eckley et al. (2010) reference. The chapter

99   "Conclusions and study implications" is written as if there were no problems.

100   Response: Following the reviewer's suggestion, we have deleted the text about the estimate of whole

101   ecosystem Hg flux in the last section.

102

103   ***Comment 8:***

104   Line 185: soil organic matter (SOM)

105   Response: The text has been changed accordingly on line 206.

106

107   ***Comment 9:***

108   Line 194: Sampling TGM in pore air is mentioned – how was it made? What were the results?

109   Response: We sampled the TGM in the soil pore gas as part of this study, but not the results are on

110   presented in this paper.   Initially we wanted to combine the DFC measurements with the soil pore

111   Hg results in a single comprehensive paper, but the reviewers felt this was too much material for a

112   single paper. So we have split the results into two papers: this paper with the DFC results and a

113   companion paper summarizing the soil Hg gas patterns. The companion manuscript on TGM

114   concentrations in the pore gas has been submitted to another journal. However we would like to

115 make linkages between the two data sets and therefore have brought the soil pore Hg data into the

116 discussion in this manuscript in Fig. S10 and S11 and line 467-470:

117 "In a companion study, the soil pore TGM concentrations were measured at all the plots at the

118 subtropical and temperate forests, except the wetlands (Zhou et al., in review). These results showed

119 that gradient of TGM concentrations between the surface air and pore air at 3 cm were significantly

120 correlated with the soil-air TGM fluxes at all the plots (Fig. S11 and S12)."

121

122

123 **Fig. S11.** Correlations between the gradient of Hg(0) concentrations between surface soil pore (at 3

124 cm) and atmosphere values and soil-air TGM flux at four plots at the subtropical forest.
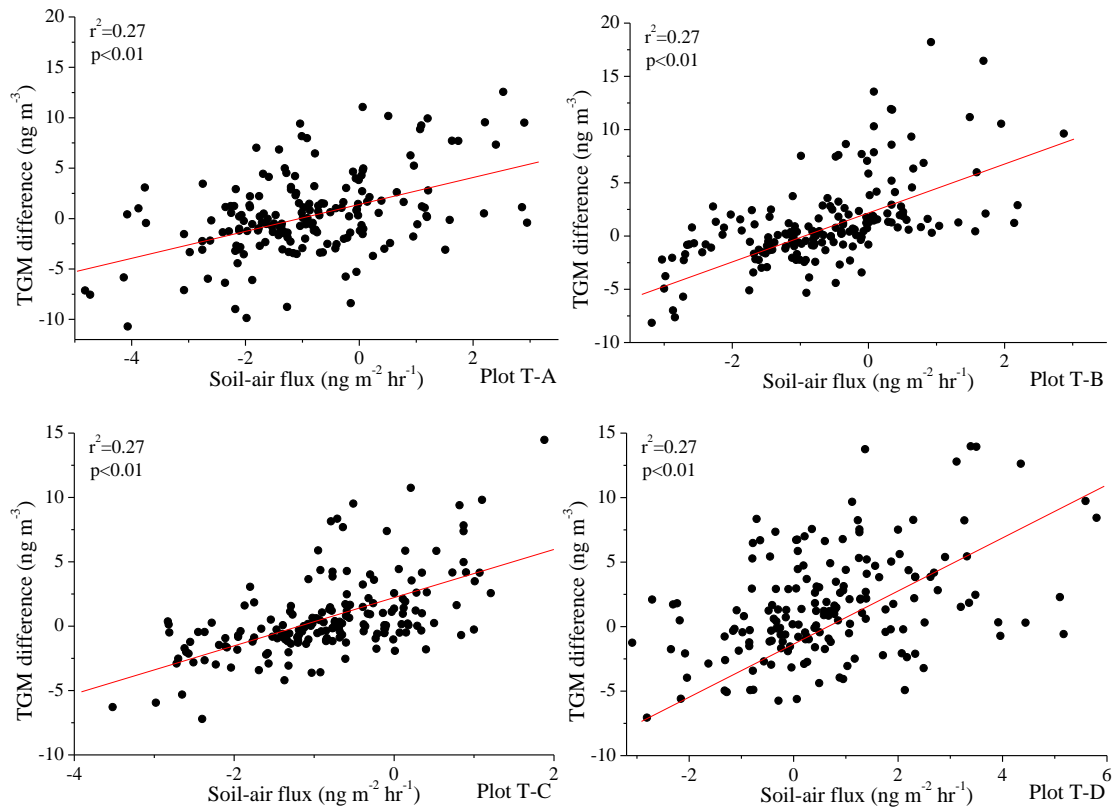
125
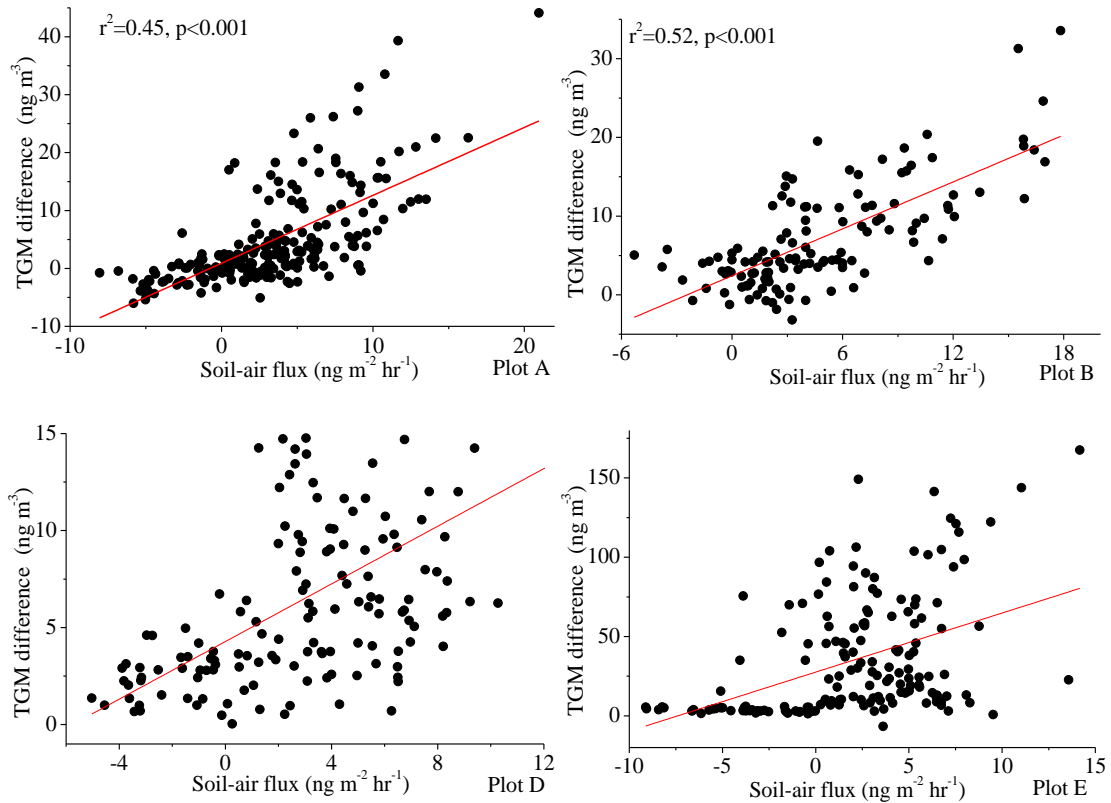
Fig. S12. Correlations between the gradient of Hg(0) concentrations between surface soil pores at (3 cm) and atmosphere values and soil-air TGM flux at four plots at the temperate forest.

Comment 10:

Line 267: were

Response: The text has been revised accordingly.

Comment 11:

Lines 273-279: The influence of soil humidity is discussed here only in terms of physicochemical terms. It is well known that microbiological processes in dry soils are greatly enhanced by occasional precipitation.

Response: We have added the text to the discussion about microbiological processing of Hg in line 301-305:

"Additionally, given that Hg conversion to Hg(0) in soil profiles occurs mainly via biotic processes, maximum aerobic microbial activity has been delineated at soil water content equivalent to 60% of a soil's water holding capacity (Breuer et al., 2002;Kiese and Butterbach-Bahl, 2002).

6

Appropriate soil moisture in the wetland would likely enhance the microbial reduction of Hg(II) to

Hg(0)."

Comment 12:

Line 296: "physicochemical properties" – what about microbiological ones?

Response: We have added the microbial community in the sentence in line 322-325:

"The forest canopy not only influences the soil Hg concentration by mediating atmospheric Hg

deposition (Zhou et al., 2018;Zhou et al., 2017), but also alters soil physio-chemical properties (e.g.

SOM, pH, porosity) (Mo et al., 2011) and microbial communities (Nagati et al., 2020), which affect

soil-air exchange."

Comment 13:

Line 368: Photo-reduction of Hg2+ may be a major driver in waters but hardly in soils which

are impenetrable to solar radiation. More plausible is the explanation by higher soil temperature and

the related higher microbiological activity.

Response: We agree with the reviewer. We have changed the text to "soil water Hg(II) to volatile

Hg(0)" in line 400.

Additionally, we have also highlighted the role of biotic processes in soil Hg(0) emissions in line

424-428:

"The Hg(0) in soil pore gas mainly results from biotic production. For example, soil sterilization

can decrease Hg converted to Hg(0) by ~50% ; additionally, 1% of the soil Hg is converted to Hg(0)

via abiotic processes, compared to 6.8% by biotic processes at 283 K, and the fraction of Hg

reduction by biotic processes increases with temperature increases (Pannu et al., 2014)."

Comment 14:

Paragraph, lines 417-433, Figure 5: Are these correlations made with data from all seasons? I

would expect different compensation points for different seasons.

Response: Yes, the correlations were made with data from all seasons.

Comment 15:

Figures 3 and 4: What does the x axis mean?

Response: the x axis means date, and we have added "date" in all the subfigures.

Comment 16:

Figures 5 and 6: Are these plots seasonally resolved? If not please state that data from all seasons were used.

Response: The data include all four seasons in each plot. We have added the note to this effects in the captions.

Comment 17:

SI, "Environmental measurements": The measurements of soil temperature (depth) is not mentioned here and neither in "Experimental". This parameter is the crucial one for physicochemical and microbiological processes in the soil. According to Figure S6 it seems to have been measured. I would prefer to discuss all relationships in relation to soil temperature instead of solar radiation. Solar radiation is essentially only a sort of proxy parameter for soil temperature. It is also not applicable for the night.

Response: Yes, we have measured the soil temperature by TDR in line 61-63:

"Soil percent moisture and soil temperature at 0-5 cm was monitored with Time Domain Reflectometry (TDR) Hydra Probe II (SDI−12/RS485) and a Stevens water cable tester (USA)."

Following the reviewer's suggestion, we have added some of discussion related to effects of soil temperature on Hg(0) emissions. Additionally, we have also added structural equation modeling (SEM) (Fig. 5) to evaluate the dominate factors controlling the soil-air Hg exchange flux. The results of this analysis shows that temperature is the main factor driving Hg evasion from forest soils.

Comment 18:

SI, description of MDL: Any information about the Hg content of litterfall and soil?

Response: We have litterfall and soil data in Chinese pine, larch, and deciduous broadleaved forest. We have added text to this effect on line 53-56 in the SI:

"From previous studies, the mean litterfall Hg concentrations were 15.8, 19.6, and 12.1 ng g^{-1} in Chinese pine forest, larch forest, and mixed broad-leaved forest plots and the mean soil Hg

204 concentrations (0-5 cm) were 72±12, 141±15, and 74±9 ng g^{-1} in Chinese pine forest, larch forest,

205 and mixed broad-leaved forest, respectively (Zhou et al., 2017)."

206

207 **Soil-atmosphere exchange flux of total gaseous mercury (TGM) at subtropical**

208 **and temperate forest catchments**

209

210 Jun Zhou [a, b, c, f], Zhangwei Wang [a, c, *], Xiaoshan Zhang [a, c], Charles T. Driscoll [d], Che-Jen Lin [e]

211

212 a. State Key Laboratory of Urban and Regional Ecology, Research Center for Eco-Environmental

213   Sciences, Chinese Academy of Sciences, Beijing 100085, China.

214 b. Key Laboratory of Soil Environment and Pollution Remediation, Institute of Soil Science,

215   Chinese Academy of Sciences, Nanjing 210008, China.

216 c. University of Chinese Academy of Sciences, Beijing 100049, China.

217 d. Department of Civil and Environmental Engineering, Syracuse University, 151 Link Hall,

218   Syracuse, New York 13244, United States.

219 e. Center for Advances in Water and Air Quality, Lamar University, Beaumont, Texas 77710,

220   United States.

221 f. Department of Environmental, Earth and Atmospheric Sciences, University of Massachusetts,

222   Lowell, 01854, USA

223

224 * Corresponding author: Zhangwei Wang

225 E-mail address: wangzhw@rcees.ac.cn (Z. Wang); Phone: +86 10 62849168.

226 No.18 Shuangqing Road, Beijing 100085, China

227

228 First author e-mail: zhoujun@issas.ac.cn (J. Zhou); Phone: +86 25 86881319.

229 No.73 East Beijing Road, Nanjing 210008, China.

230

Abstract: Evasion from soil is the largest source of mercury (Hg) to the atmosphere from terrestrial ecosystems. To improve understanding of controls and in estimates of forest soil-atmosphere fluxes of total gaseous Hg (TGM), measurements were made using dynamic flux chambers (DFC) over 130 and 96 days for each of five plots at a subtropical forest and a temperate forest, respectively. At the subtropical forest the highest net soil Hg emissions were observed for an open field (24 ± 33 ng m^{-2} hr^{-1}), followed by two coniferous forest plots (2.8 ± 3.9 and 3.5 ± 4.2 ng m^{-2} hr^{-1}), broad-leaved forest plot (0.18 ± 4.3 ng m^{-2} hr^{-1}), and the remaining wetland site showing net deposition (-0.80 ± 5.1 ng m^{-2} hr^{-1}). At the temperate forest, the highest fluxes and net soil Hg emissions were observed for a wetland (3.81 ± 0.52 ng m^{-2} hr^{-1}) and an open field (1.82 ± 0.79 ng m^{-2} hr^{-1}), with lesser emission rates in deciduous broad-leaved forest (0.68 ± 1.01 ng m^{-2} hr^{-1}) and deciduous needle-leaved forest (0.32 ± 0.96 ng m^{-2} hr^{-1}) plots, and net deposition at an evergreen pine forest (-0.04 ± 0.81 ng m^{-2} h^{-1}). High solar radiation and temperature during summer resulted in the high Hg emissions in the subtropical forest, and the open field and evergreen pine forest at the temperate forest. At the temperate deciduous plots, the highest Hg emission occurred in spring during leaf-off period due to direct solar radiation exposure to soils. Fluxes showed strong positive relationships with solar radiation and soil temperature, and negative correlations with ambient-air TGM concentration in both subtropical and temperate forests, with area-weighted compensation points of 6.82 and 3.42 ng m^{-3}, respectively. The values of the compensation points suggest that the atmospheric TGM concentration can play a critical role in limiting TGM emissions from the forest floor. Climate change and land-use disturbance may increase the compensation points in both temperate and subtropical forests. Future research should focus on the role of legacy soil Hg in reemissions to the atmosphere as decreases in primary emissions drive decreases in TGM concentrations and disturbance of climate change and land use.

Keywords: soil-air flux of total gaseous mercury; dynamic flux chamber; compensation point; climate change; land use

1. Introduction

Mercury (Hg) is a persistent, bio-accumulative, toxic and well-established global contaminant (Obrist et al., 2018). Unlike other trace metals in the atmosphere, the Hg mainly exists as gaseous elemental Hg (Hg(0)), which accounts more than 90% of total gaseous Hg (TGM). Hg(0) is relatively inert and has a long atmospheric lifetime of 0.5–1 year, which allows for long range transport (Kamp et al., 2018;Slemr et al., 2018;St Louis et al., 2019). Global long-range atmospheric transport and deposition is the main pathway of Hg input to remote ecosystems (Lin et al., 2019;Ly Sy Phu et al., 2019;Sun et al., 2019). Soils account for more than 90% of Hg stored in terrestrial ecosystems (Obrist, 2012), with global top soil Hg pools (0–40 cm) estimated at > 300 000 Mg (Hararuk et al., 2013;Zhou et al., 2017a). The large soil Hg pools not only stem from geologic sources, but also from a legacy of historically anthropogenic emissions over the centuries (Obrist et al., 2014;Du et al., 2019).

Although many studies have focused on primary anthropogenic Hg emissions, releases from natural source materials is also an important pathway but with greater uncertainty and variability, including emissions from natural reservoirs (e.g. volcanic activity, geothermal sources, weathering of Hg from soil minerals) and re-emissions of previous deposited Hg. These natural sources can be equal to or two-fold larger than anthropogenic sources (Outridge et al., 2018;Fraser et al., 2018). Recent global Hg models estimate that 3600 Mg yr^{-1} of atmospheric Hg is deposited to terrestrial surfaces, with 1000 Mg yr^{-1} re-emitted back to the atmosphere (Outridge et al., 2018). Moreover, compared to primary anthropogenic emissions of Hg (2500 Mg yr^{-1}), estimates of re-emissions from soil surfaces are highly uncertain (Outridge et al., 2018;Wang et al., 2018). Compiling data from 132 studies, Agnan et al. (2016) found that the Earth's surface (particularly in East Asia) is an increasingly important source of total gaseous Hg (TGM) emissions, with up to half of the global emissions derived from natural sources. They estimated terrestrial TGM emissions of 607 Mg yr^{-1}, but with a large uncertainty range of −513 to 1353 Mg yr^{-1}. Additionally, a recent review suggests that future research should focus on campaigns to understand forest Hg behavior and long-term Hg observations, particularly in Asia (Zhang et al., 2019b).

Forest soils receive Hg inputs from: 1) throughfall that include wet deposition plus the wash off of Hg (II) deposited on foliage surfaces; 2) litterfall that contains foliage and other plant materials that have assimilated atmospheric Hg(0); and 3) direct dry Hg deposition to soil from the atmosphere

(Teixeira et al., 2018;Risch et al., 2017;Olson et al., 2018;Cheng et al., 2020). Mercury outputs from forest soils occur from surface or subsurface runoff and air-land surface evasion. Forest soils are highly complex media, with important features that affect soil-air exchange, including soil physio-chemical characteristics (e.g., porosity, oxygen availability, redox potential, organic matter, pH) (Obrist et al., 2010;Carpi et al., 2014). Other factors also influence this process, such as meteorological conditions (e.g., solar radiation, air temperature, precipitation) (Zhou et al., 2015;O'Connor et al., 2019), atmospheric chemistry (ozone, nitrate and hydroxyl radicals) (Peleg et al., 2015;Angot et al., 2016), atmospheric TGM concentrations (Wang et al., 2007) and biological processes (Obrist et al., 2010;Chen et al., 2017). Therefore, to characterize and quantify land-atmosphere exchange of TGM, it is necessary to understand the roles of these factors in mediating this process.

Field studies have shown that elevated anthropogenic Hg emissions in South-East Asia have resulted high atmospheric Hg concentrations an deposition regionally (Kumari et al., 2015;Pan et al., 2010;Zhang et al., 2019b). Forests experience particularly elevated net Hg loads due to enhanced deposition associated with the tree canopy, especially in China (Wang et al., 2016;Zhang et al., 2019a). The annual loading of THg to subtropical forests in China have been shown to be much higher than forest catchments in Europe and North America (Wright et al., 2016;Zhou et al., 2020). High Hg deposition has resulted in elevated soil Hg pools in Chinese subtropical forests (Wang et al., 2018;Wang et al., 2009). In contrast, a recent study showed that the Hg deposition and soil Hg concentrations at a temperate forest in China were similar to those in Europe and North America (Zhou et al., 2020). The forested area in China is 2.2×10^4 km^2, with about 50% and 40% occurring in subtropical and temperate zones, respectively. Therefore, it seems likely that subtropical and temperate forests in China, with contrasting climate, vegetation cover, and atmospheric Hg deposition, may also show different patterns of Hg cycling.

Forest ecosystems not only act as sinks for atmospheric Hg deposition, but can also serve as sources resulting from legacy Hg that has accumulated in surface soil. For example, one study constructed the Hg budget in subtropical forest in southern China showing that the forest is a minor sink for atmospheric Hg but a significant net Hg(0) source (58.5 μg m^{-2} yr^{-1}) (Yu et al., 2020). In contrast, another study also in southern China using budgets of air-foliage and air-soil Hg(0) exchange fluxes, showed that forest is a net sink of Hg(0) (20.1 μg m^{-2} yr^{-1}) (Yuan et al., 2019a;Yuan

There has been much research characterizing Hg fluxes between the forest floor and the atmosphere from studies worldwide, as reviewed by Zhu et al. (2016) and Agnan et al. (2016). In this paper, we present measurements on atmosphere-land Hg fluxes conducted over 130-days and 96-days, respectively, during four seasons for five sites both at a temperate forest catchment at Mt. Dongling (MDL) and a subtropical forest catchment at Tieshanping Forest Park (TFP) in China. The aims of this investigation were to (1) characterize the air-land surface Hg fluxes in different terrestrial ecosystems; (2) conduct detailed field measurements to characterize the uncertainty of land use and climate change in air-surface fluxes of TGM in forest catchments; and (3) to compare estimates of Hg emissions from forest soils at temperate and subtropical zones. We hypothesize that a multi-plot and multi-seasonal study of soil-air fluxes in each forest system will provide new perspectives on the climate change and land use on the soil-air Hg fluxes, and improve understanding and estimates of soil Hg evasion from forest ecosystems.

2. Materials and methods

2.1. Study area

This study was conducted at TFP in the subtropical zone (106°41.24′E, 29°37.42′N) and at MDL in the temperate zone (115°26′, E40°00' N) in China (Fig. 1). The TFP is dominated by a Masson pine (*Pinus massoniana* Lamb.) stand (conifer) with some associated species, such as camphor (*Cinnamom camphora*) and Gugertree (*Schima superba* Gardn), which were planted in 1960s following the loss of a natural Masson pine forest. The forest is located about 20 km northeast of Chongqing City, at an altitude from 200 to 550 m. The mean annual precipitation is 1028 mm, with 75% of the rainfall occurring from May to October. The mean annual air temperature is 18.2 °C. The total area of the study forest in the TFP is 1.06×10^3 ha. The soil is typically mountain yellow earth (corresponding to an Acrisol in the FAO) (FAO, 1988), with clay mineralogy dominated by kaolinite (Zhou et al., 2016).

Mt. Dongling is near the Beijing Forest Ecosystem Research Station, Chinese Academy of Sciences, which is located 110 km southwest of mega-city Beijing in North China. The elevation is

14

1300 m asl. The annual average rainfall is 612 mm and mean relative humidity is 66%. The climate of the region is predominantly warm temperate continent monsoon with an annual average temperature of 4.8 °C and precipitation of 611.9 mm. Soil type is mountain brown earth (corresponding to a Eutric cambisol in FAO) (FAO, 1988) (Zhou et al., 2018). The relatively cool climate in the study area has resulted in deep litter and high organic matter concentrations (Fang et al., 2007). The study area is a mature, secondary forest protected since the 1950s following the extensive deforestation. Hg concentrations in environmental media at the site are provided in the Supporting Information (SI, Supporting Text).

2.2. Dynamic flux chamber (DFC) measurement

To reduce the spatial uncertainty in Hg fluxes, different ecosystems were selected for study in a sub-catchment at the subtropical TFP, including a coniferous forest (plots S-A and S-B), a wetland (plot S-C), a broad-leaved (camphor) forest (plot S-D) and an open field with bare soil (plot S-E), and a sub-catchment at the temperate MDL, including a Chinese pine forest (plot T-A), larch forest (plots T-B), wetland (plots T-C), mixed broad-leaved forest (plots T-D) and open field (plots T-E) (Fig. 1). To reduce temporal uncertainty in Hg fluxes, 130-days and 96-days of flux observations were undertaken over four seasons (about one-month of continuous observations for each season, except for one-week during winter at the MDL) (Table S1). The locations of each plot is described in the Table 1 and illustrated in Fig. 1.

Semi-cylindrical quartz glass and open-bottom DFCs (4.71 L) were utilized during the sampling campaign. The area of the DFCs over the soil surface was 20 × 30 cm, with six inlet holes (1 cm diameter) (Fig. S1). Local fine grained soil was placed outside the chamber to seal any gap between the base of the chamber and the soil. At the outlet of the chamber, an orifice was connected to two exit tubes: one to a regulated suction pump and the other to a gold cartridge for trapping outlet TGM. A sub-stream of air was trapped by a pair of gold quartz cartridges at a flow rate of 0.5 L min^{-1}, which was measured using an integrating volume flow meter. All the gold cartridges were constructed with gold silk (< 0.5 mm diameter). The strands of gold silk were rolled together in a small coil and about 15 coils were used to fill a quartz cartridge with about 2 g of gold. The accuracy of all traps were evaluated (see section 2.4) and non-conforming cartridges were discarded. The chamber flushing flow turnover time (TOT) was 0.47 min and 0.94 min for the subtropical forest

and temperate forest plots, respectively. The Hg flux was calculated using the following equation:

$$F = (C_0 - C_i) \times Q/A$$

where F is the soil Hg flux (ng m^{-2} hr^{-1}); C_o and C_i are the steady state Hg concentrations (ng m^{-3}) of the outlet and inlet air streams, respectively, which were calculated by the Hg mass detected in gold cartridges and the corresponding air volume; A is the surface area enclosed by the DFC; Q is the flow rate of ambient air circulated through the DFC (10 L min^{-1} for TFP and 5 L min^{-1} for MDL).

High flow rates and short TOTs are appropriate for measuring flux from soils with high Hg concentrations or emissions, while lower flow rates and longer TOT are more appropriate for soils with low Hg concentrations or emissions. Eckley et al. (2010) suggested that the optimal flow was at the beginning of the stable $C_0 - C_i$ (ΔC) period, which was chosen as a compromise between competing criteria aimed at creating conditions inside the DFC similar to the adjacent outside air. Our previous study showed that when ΔC was relative stable, the corresponding flushing flow rate was from 5 to 10 L min^{-1} at the subtropical forest (Zhou et al., 2017a). To avoid suppression of Hg emissions due to the excessive buildup of Hg within the chamber, the flow rate of ambient air circulated through the DFC was 10 L min^{-1} at the subtropical forest. At the temperate forest, the soil Hg concentrations was about 3-4 times lower than those at the subtropical forest, so the lower flow rate of 5 L min^{-1} was used at these plots. The DFC chambers in all plots were moved every week to mitigate against changes in soil moisture due the covering of soil by the chambers. If a precipitation event occurred, the chambers were also moved to new positions during the sampling period (morning or evening) to be representative of soil conditions receiving ambient precipitation.

The pair of gold cartridges for each DFC were collected twice a day: every morning (about 8:00) and afternoon (about 17:00) representing night (17:00−8:00 of next day) and day (8:00−17:00) emissions, respectively. Twenty gold quartz cartridges were alternated during the sampling program. In addition, diurnal variations of soil-air Hg fluxes were also conducted in each season, with gold cartridges collected every half an hour. A total of four diurnal measurements were conducted over the study in each forest, with diurnal variations were measured one day per season. It has been reported that the DFC measurements can introduce bias under a given design flushing air flow rates and environmental condition (Lin et al., 2010;Zhang et al., 2002). The DFC enclosure imposes a physical constraint that can lead to accumulation in or evasion from the soil surface under measurement. Extensive experiments were conducted at our plot sites to determine the appropriate

407 experimental conditions for accurate measurements. We followed recommendations made by

408 Eckley et al. (2010) for our measurements.

409

410 **2.3. Environmental measurements**

411 At each sampling plot, soil samples were collected from the DFC footprint (0−5 cm). Soil Hg

412 and soil organic matter (SOM) concentrations were measured using a DMA-80 direct Hg analyzer

413 (Milestone Ltd., Italy) and loss on ignition (LOI) method, respectively, using methods detailed in

414 the SI. Soil percent moisture and temperature were monitored with Time Domain Reflectometry

415 (TDR) Hydra Probe II (SDI−12/RS485) and a Stevens water cable tester (USA). Solar radiation was

416 measured by a weather station (Davis Wireless Vantage VUE 06250 Weather Station, Davis

417 Instruments, Hayward, CA) located in the TFP Forest Station and Beijing Forest Ecosystem

418 Research Station, within about 500 m of each plot.

419

420 **2.4. Quality assurance and quality control (QA/QC)**

421 All cartridges were transported to a laboratory at the TFP Forest Station for Hg determination

422 using a cold vapor atomic fluorescence spectroscopy (CVAFS) detector (Brooks Rand III). The limit

423 of detection, based on three times the standard deviation of replicate measurements of the blank was

424 1 pg. Based on the sampled air volume, the detection limits were < 0.10 ng m^{-3}. A calibration curve

425 was developed using Hg saturated air and the calibration curve was required to have a correlation

426 coefficient greater than 0.99 before the samples analysis could proceed. Before and after the

427 measurement of the sampling cartridges in each day, standard Hg saturated air was injected to test

428 the accuracy of the Hg analyzer. If the deviation of the measured Hg mass was higher than 5%, new

429 calibration curve would be developed.

430 A controlled volume of saturated Hg air at a known temperature was injected to measure Hg

431 recovery from the gold cartridges before and after the campaigns in each season. The recoveries of

432 gold cartridges before and after the operation ranged from 98.8 to 103.2% and 96.3 to 102.5%

433 (n=155, average=98.9%), respectively. The collection efficiency of Hg vapor by the gold cartridges

434 was determined by connecting two cartridges in sequence and sampling the ambient air over 24 h

435 in the laboratory. For all cartridges, less than 1% Hg was detected on the second cartridges compared

436 to the first cartridge, indicating that more than > 99% of TGM was absorbed by the gold cartridges

437   during the field operation. For comparison, Hg fluxes were measured by two chambers side by side

438   simultaneously. Blanks of the soil TGM flux sampling systems were measured by placing the DFC

439   on a quartz glass surface in the five plots. The sampling time for blank measurements was same as

440   soil-air TGM flux measurements, which were collected at 8:00 and 17:00, representing night

441   (17:00−8:00 of next day) and day (8:00−17:00) emissions, respectively. The averaged blank was

442   0.13 ± 0.21 ng m^{-2} h^{-1} (n=10), which was subtracted from the soil-air TGM flux for each season.

443

444   **2.5. Statistical analysis**

445   Structural equation modeling (SEM) were performed on the collected Hg flux data using Amos

446   software. SEM, developed from a fully conceptual model using χ2 tests with maximum likelihood

447   estimation, was conducted to infer the interplay of temperature, solar radiation, soil moisture, and

448   air TGM concentrations on measurements of soil-air TGM exchange fluxes. Seasonal and annual

449   fluxes were compared among the ten plots. Separate two-way ANOVAs were used to determine if

450   differences in Hg fluxes existed among the seasons and sites. All differences in mean values were

451   significant at the p=0.05 level and all means are reported with ± one standard deviation from the

452   mean. The correlations between environmental parameters and fluxes were analyzed by Pearson's

453   Correlation Tests using SPSS software (SPSS Inc. 16.0) and correlation coefficient and p values are

454   presented and significantly correlated at the level of 0.05.

455

456   **3. Results and discussion**

457   **3.1. Landscape- and forest species-dependence of soil-air Hg fluxes at the forest catchment**

458   **scale**

459   The soil TGM flux measurements for the five plots were calculated for the day and night and

460   reported as mean daily fluxes with standard deviations (SD) at the subtropical (Fig. 2a) and

461   temperate forests (Fig. 2b). Over the course of the campaigns, net TGM emission was observed at

462   the open field (24 ± 33 ng m^{-2} hr^{-1}), coniferous forest (upper elevation 2.8 ± 3.9 ng m^{-2} hr^{-1}, mid

463   elevation 3.5 ± 4.2 ng m^{-2} hr^{-1}) and the broad-leaved forest (0.18 ± 4.3 ng m^{-2} hr^{-1}), while net

464   deposition was evident at the wetland (-0.80 ± 5.1 ng m^{-2} hr^{-1}), respectively, at the subtropical

465   forest. At the temperate forest, net TGM emission was observed at the wetland (3.81 ± 0.52 ng m^{-2}

466   hr^{-1}), open field (1.82 ± 0.79 ng m^{-2} hr^{-1}), mixed broad-leaved forest (0.68 ± 1.01 ng m^{-2} hr^{-1}),

467   larch forest (0.32 ± 0.96 ng m^{-2} hr^{-1}), while net deposition was evident at the Chinese pine forest

468   (-0.04 ± 0.81 ng m^{-2} h^{-1}), respectively. The fluxes at the temperate forest were 10-times lower than

469   values at the subtropical forest due to different environmental factors, such as lower temperature,

470   solar radiation and soil Hg concentrations (see section 3.3).

471   These patterns suggest that soil-air Hg fluxes at catchment scale vary by soil properties (e.g.,

472   soil Hg concentration, moisture, SOM) and forest species composition. High variability, as

473   evidenced by high SD and coefficient of variation (SD/mean, range of 14−2374%), was evident in

474   daily Hg fluxes largely driven by meteorological variation. The fluxes at the subtropical forest

475   plots of this study were much lower than those reported for other subtropical evergreen forests in

476   China such as Mt. Gongga (0.5–9.3 ng m^{-2} hr^{-1}) (Fu et al., 2008), Mt. Jinyun (14.2 ng m^{-2} hr^{-1})

477   (Ma et al., 2013) and Mt. Simian (11.23 ng m^{-2} hr^{-1}) (Ma et al., 2018), all of which were generally

478   conducted during sunny days. Our flux measurements at temperate forest were slightly lower or

479   comparable to those in North American deciduous forests, ranging from −0.73 to 2.7 ng m^{-2} hr^{-1}

480   (Choi and Holsen, 2009b;Hartman et al., 2009;Carpi et al., 2014;Ma et al., 2018). These results

481   demonstrated that measurements over several days may exhibit considerable temporal variability

482   and long-term study should be undertaken to reduce the uncertainty in temporal patterns of soil Hg

483   emissions.

484   The mean TGM fluxes in the open fields were about 10 and 6 times higher than those under

485   the forest canopy at the subtropical and temperate forests, respectively ($p < 0.001$). Our results are

486   consistent with Ma et al. (2013) and Xin and Gustin (2007), showing large Hg evasion following

487   forest conversion to bare soils due to direct exposure to sunlight, as fluxes were enhanced by

488   increases in solar radiation and temperature. Due to frequent heavy rains at the subtropical forest

489   catchment, a large amount of surface runoff impacted the wetland (plot S-C). Elevated runoff may

490   have decreased Hg (96 ± 43 ng g^{-1}) and SOM in surface soils due to erosion (Table 1). This site had

491   the lowest TGM fluxes of the plots studied at the subtropical forest (overall net sink). In addition,

492   soils in the wetland plot were mostly saturated throughout the year, limiting Hg fluxes and likely

493   contributing to the sink behavior. In contrast, the mean annual rainfall was 40% lower at the

494   temperate forest and the wetland was located at relatively lower terrain. Litter from surrounding

495   higher terrain forest accumulated in the low lying wetland. The cool and dry climate also contributed

496   to high organic matter and low bulk density (Fang et al., 2007). Higher SOM likely facilitated

binding of trace metals, leading to high soil Hg concentrations (117 ng g^{-1}) at the temperate wetland. These conditions were conducive to biological activity, promoting the mineralization of SOM and the release of volatile Hg(0) from soil (Choi and Holsen, 2009b;Osterwalder et al., 2019). The wetland had the highest TGM fluxes of the plots studied at the temperate forest (overall net source). Previous studies have suggested that soil water is able to mobilize Hg from binding sites on soil (Gustin, 2003;Kocman and Horvat, 2010) and high soil water decreases soil redox potential (Zarate-Valdez et al., 2006), both of which can facilitate the conversion of Hg(II) to Hg(0). Additionally, the climate is relatively dry in north China, especially in spring. The high solar radiation and relatively high air temperature not only enhance the reduction of Hg(II) to Hg(0), but also increase water evaporation compared to other study sites. Enhanced water evaporation at higher temperature, facilitates Hg emissions from soils (Gustin and Stamenkovic, 2005;Lin et al., 2010). Additionally, given that Hg conversion to Hg(0) in soil profiles occurs mainly via biotic processes, maximum aerobic microbial activity has been delineated at soil water content equivalent to 60% of a soil's water holding capacity (Breuer et al., 2002;Kiese and Butterbach-Bahl, 2002). Appropriate soil moisture in the wetland would likely enhance the microbial reduction of Hg(II) to Hg(0). Therefore, the highest Hg flux was observed in the temperate wetland, especially in spring. The main reasons for the significant differences between the soil Hg fluxes at the two wetland sites is likely that the saturated soil at the subtropical forest inhibited Hg(0) evasion (Gustin and Stamenkovic, 2005) (see section 3.3).

At the subtropical forest, litterfall in the broad-leaved (camphor) plot (plot S-D) was twice as high as that of the coniferous (pine) plot (plots S-A and S-B) (Zhou et al., 2018), likely resulting in greater shielding of sunlight to the surface soil and limiting soil Hg evasion. Increases in light transmission through the canopy increase both solar radiation and soil temperature, which can enhance photochemical reduction of Hg(II) at the soil surface and Hg(0) evasion. In the mid-slope of the pine stand (plot S-B), soil Hg concentration was elevated compared to the upslope plot (Table 1), with corresponding with higher soil Hg fluxes. At the temperate forest, the lowest Hg flux and overall deposition was observed at the evergreen forest of Chinese pine, where the canopy cover likely limited Hg flux by decreasing solar radiation to soil and warming. Similar at the subtropical forest, the needle biomass in the larch plot was about 2.5 times greater as that in the mixed broad-leaved plot (plot T-D) at the temperate forest, resulting in shielding the sunlight to the surface soil

527   and limiting soil Hg evasion at larch plot.

528   The forest canopy not only influences the soil Hg concentration by mediating atmospheric Hg

529   deposition (Zhou et al., 2018;Zhou et al., 2017a), but also alters soil physio-chemical properties (e.g.

530   SOM, pH, porosity) (Mo et al., 2011) and microbial communities (Nagati et al., 2020), which affect

531   soil-air exchange. For example, the annual litterfall Hg deposition flux at the broad-leaved plot (91

532    $\mu g\ m^{-2}\ yr^{-1}$) at the subtropical forest was approximately two times greater than the coniferous plot

533   (41 $\mu g\ m^{-2}\ yr^{-1}$) (Zhou et al., 2018). Conversely, the SOM and soil Hg concentrations in the broad-

534   leaved forest were lower than the coniferous forest. Moreover, litter decomposition rate was lower,

535   but the Hg mass accumulation in the litter was much higher in the coniferous forest compared to the

536   broad-leaved forest due to higher throughfall Hg deposition at the coniferous plot (Zhou et al., 2018),

537   which resulted in a seemingly inconsistent pattern between litterfall mass and SOM, as well as

538   litterfall Hg deposition and soil Hg concentrations. At the temperate forest, the higher litterfall Hg

539   deposition and lower litter decomposition in the larch plot compared to the broad-leaved plot (Zhou

540   et al., 2017a), resulted in significant higher SOM and soil Hg concentrations (Table 1). Tree species

541   can change the physicochemical properties of soil (e.g. SOM, soil Hg concentrations) and influence

542   soil-air exchange. These biological factors likely contribute to the much lower TGM evasion in the

543   broad-leaved plot than the coniferous plot at the subtropical forest, but much higher TGM evasion

544   in the broad-leaved plot than the deciduous needle (larch) plot at the temperate forest (Fig. 2).

545   Most studies measure soil TGM fluxes at only one location or at a single forest stand to

546   characterize the whole ecosystem. Our observations clearly show that soil-air Hg fluxes vary

547   substantially across different plots (Fig. 2), indicating that forest type/cover and landscape position

548   significantly affect the TGM fluxes and therefore the spatial variability in soil Hg fluxes among

549   different sub-plots must be considered. Based on the areal distribution of each plot type in the study

550   sub-catchments of the subtropical forest (coniferous upland and mid-slope, broad-leaved, wetland,

551   open) (4.6 ha) and the temperate forest (Chinese pine, larch, wetland, mixed broad-leaved and

552   open) (5.0 ha) (Table S1), the area-weighted TGM flux was 3.2 and 0.32 $ng\ m^{-2}\ hr^{-1}$ for the entire

553   subtropical and temperate catchments, respectively. The area-weighted TGM fluxes were 14%

554   higher than plot S-A and 16% lower than plot S-B of the Masson pine stand at the subtropical

555   forest, and were 907% higher than Chinese pine plot and 53% lower than mixed broad-leaved plot

556   at the temperate forest, respectively. The observations at several plots with diverse forest cover in

557   this study should reduce the overall uncertainty associated with soil-air fluxes of TGM in the

558   overall forest catchment.

559

560   **3.2. Seasonal variations of soil-air Hg fluxes at the forest catchment scale**

561   Soil TGM fluxes not only exhibited clear seasonal variations at all the plots, but also were

562   responsive to phenological and meteorological patterns. At the subtropical forest, soil Hg fluxes

563   were generally highest in the summer (Fig. 2a), which showed net emissions at all the five plots,

564   followed by spring and autumn, with the lowest values during winter, which exhibited net deposition

565   at all plots with the exception of plot S-B. The observed seasonal variation was dependent on

566   sunlight (Fig. 3), because solar radiation drives photochemical reduction of Hg(II) (note the

567   correlation between the TGM fluxes and solar radiation, Fig. S2). Additionally, greater solar

568   radiation increases temperature, which promotes the production of soil Hg gas by biological and

569   abiotic processes. At the temperate forest, the Hg fluxes were the highest in the deciduous forest

570   plot (wetland, mixed broad-leaved forest and larch forest) in spring before leaf-out when solar

571   radiation could directly reach the forest floor (Fig. S3). In the open field and evergreen forest

572   (Chinese pine forest) plots, the Hg fluxes were highest in summer with the highest solar radiation

573   and temperature (Fig. 4 and Fig. S3). The lowest Hg fluxes were measured in the winter at all plots

574   when the soil was covered with snow, with net Hg emission observed at the open field and net

575   deposition observed at the other four sites (Fig. 2b).

576   We also observed strong variation in TGM evasion under different weather conditions. Rain

577   events decreased TGM fluxes at all plots in both forests (Fig. S4), as the rainwater decreased soil

578   pore space leading to decreases in evasion from soil. Furthermore, the solar radiation and

579   temperature during rainy days was much lower than those for sunny days for a given season (Fig. 3

580   and Fig. 4). Manca et al. (2013) studied snow-air Hg exchange at Ny-Ålesund, showing on average

581   a small net deposition -0.24 ng m^{-2} hr^{-1}. Likewise, overall deposition between -0.6 and -23.8 ng m^{-}

582   ^{2} hr^{-1} were observed at snow-covered agricultural areas at Northeastern China (Wang et al.,

583   2013;Zhang et al., 2013). However, some studies of snowpack have shown net Hg deposition at

584   nighttime and net emissions during daytime due to high solar radiation (Maxwell et al.,

585   2013;Spolaor et al., 2019). Empirical models suggest that most of the Hg(0) deposited to snow was

586   re-emitted back to the atmosphere (Durnford and Dastoor, 2011). During the campaigns in winter,

the solar radiation was relatively lower, which may be why net deposition occurred (Fig. 4). Additionally, refrozen ice/snow layers are characterized by elevated Hg concentrations and the deposited Hg from atmosphere could be potentially released to meltwater (Zhang et al., 2012;Perez-Rodriguez et al., 2019), which is consistent with our results that atmospheric Hg deposition could release to meltwater during snow melt. Our observations through the annual climatic cycle reduce uncertainty and bias of temporal patterns of soil-air Hg fluxes. Moreover, multi-plot observations reduce the uncertainty and bias associated with spatial variation. Together these more detailed measurements improved estimates of overall ecosystem soil Hg evasion, and confirm our hypothesis.

3.3. Correlations between environmental factors and fluxes

To investigate the correlation between soil-atmosphere fluxes and environmental factors, data over the four seasons were used. These data offer a long continuous time series for the five measurement plots in each forest (Fig. 3 and 4). According to a global database, atmospheric fluxes at Hg-enriched sites are positively correlated with substrate Hg concentrations, but this relationship is not observed at sites with lower background concentrations of soil Hg (Agnan et al., 2016). Our soil Hg fluxes were strongly correlated with soil Hg concentrations at vegetated sites (forests and wetland) at the subtropical forest (Fig. S5), but not at the temperate forest.

Photo-reduction is a major driver of TGM evasion from the Earth's surface (Howard and Edwards, 2018;Kuss et al., 2018;Gao et al., 2020). This process is due to photochemically mediated reduction that converts soil water Hg(II) to volatile Hg(0) and enhances the Hg(0) pool in soil pores (Xin and Gustin, 2007;Choi and Holsen, 2009a). Therefore, the elevated soil pore Hg(0) concentrations increased the potential for TGM diffusion from soil to the atmosphere, which drives an increase of Hg emissions from soil. At all the study sites no matter the daily average fluxes (Fig. 3 and 4), daytime fluxes (Fig. S2 and S3) were all significantly correlated with solar radiation, and the solar radiation also increased daytime fluxes compare to nighttime values (Fig. S6). In the evergreen plots of the subtropical (plots S-A, S-B, S-D) and temperate (plot T-A) forests, Hg fluxes were the most highly dependent on soil temperature compared to the solar radiation during the four seasons, likely due to evergreen canopy limiting solar radiation to the forest floor. With the consistent shade of the coniferous forest canopy, the Hg flux was highly dependent on soil surface temperature rather than solar radiation to the forest floor.

To consider synergistic effects from multiple factors, SEM was applied to infer the soil-air TGM exchange processes (Fig. 5). It is clear that temperature was a more dominant factor driving air-soil TGM exchange flux over the four seasons in the subtropical forest plots, while solar radiation was a more dominant factor at the temperate forest due to direct exposure of the forest floor to solar radiation the leaf-off seasons. At the open fields of both forests, temperature and solar radiation had a synergistic effect on soil Hg fluxes. A recent study of soil-air TGM fluxes at subtropical evergreen broadleaf forest in South China also suggested that temperature is the most important driver of air-soil TGM exchange (Yuan et al., 2019b). Therefore, we may infer that under the shade of the forest canopy, temperature is the dominant factor causing variation in TGM evasion from forest soil.

Mercury fluxes in wetlands in both forests (plots S-C and T-C) were less strongly correlated with soil temperature compared to the other plots in both forests (Fig. S7 and S8). Generally, temperature is an important factor that promotes TGM evasion after its formation from Hg(II) more by biotic than abiotic processes in soils (Pannu et al., 2014). The Hg(0) in soil pore gas mainly results from biotic production. For example, soil sterilization can decrease Hg converted to Hg(0) by ~50% ; additionally, 1% of the soil Hg is converted to Hg(0) via abiotic processes, compared to 6.8% by biotic processes at 283 K, and the fraction of Hg reduction by biotic processes increases with temperature increases (Pannu et al., 2014). At the subtropical forest, the wetland soil was largely saturated. This condition likely limited soil pore release of TGM to the atmosphere, resulting in a weaker correlation between soil temperature and Hg fluxes. Furthermore, the Hg exchange fluxes were more dependent on solar radiation and less dependent on temperature during the leaf-off period at the temperate deciduous plots; therefore, the Hg fluxes were more solar radiation-driven in the deciduous forests, especially in the wetland (Fig. S3 and S7).

During the campaign, significant negative correlations were evident between soil moisture and soil-air fluxes of TGM at the five plots at the subtropical forest ($r^2= 0.03-0.39$, $p < 0.05$ for all, Fig. S9), but there was no significant correlations with soil moisture for the temperate forest (Fig. S10). Generally there is an optimum soil moisture condition that maximizes soil TGM flux (Gustin and Stamenkovic, 2005;Lin et al., 2010;Obrist et al., 2014;Osterwalder et al., 2018;Johnson et al., 2003), which ranges from 60% to 80% of the water holding capacity of a soil (Pannu et al., 2014). A laboratory experiment using undisturbed soil collected from the our subtropical study area showed

that increasing soil moisture from 2% to 20% increased the TGM flux 80% at 24 °C (Wang et al., 2014). A second field experiment was conducted to study the effects of higher soil moisture on TGM flux at the subtropical forest, showing that increasing soil moisture gradually decreased the soil Hg emissions over the range of 31−39% (Zhou et al., 2017b). Combining the results of these experiments, the soil Hg fluxes at the subtropical forest catchment appear to increase from low values of soil moisture reaching an optimum in the range of 20-30% and then decreasing with increasing soil moisture above these values. In the current study, we observed following an extended dry period with an extended wet period enhanced the Hg fluxes in both forests; however, individual rainfall events did not enhance or decrease the Hg fluxes due to short-term increases in soil moisture and lower solar radiation associated with those events (Fig. 3 and 4). Additionally, Lin et al. (2010) observed the synergistic effects (20–30 % of additional flux enhancement) between air temperature (15 and 30 °C) and soil moisture (2.5 and 27.5 %). Perennially humid weather results in relatively high soil moisture at the subtropical forest (largely > 25% during the campaigns). Considering the relatively high bulk density and low porosity of soil at the subtropical forest (Sørbotten, 2011), soil moisture likely exceeded the optimum range for TGM evasion during the campaigns resulting in significantly negative correlations (Fig. S9). In contrast, lower bulk density and higher soil porosity would result in higher optimum range of soil moisture at the temperate forest. Moreover, the temperate forest had a large range of soil moisture (2 to 60%) in the five plots which combined with the synergistic effects of soil moisture with temperature (Lin et al., 2010), resulted in a condition where moisture was not a main driver of TGM evasion.

Soil-air Hg fluxes also showed significant negative correlations with atmospheric TGM concentrations at the ten plots at both forests ($r^2 = 0.023−0.26$, $p < 0.05$, Fig. 6 and 7), which had a greater effect than soil moisture at both forests, except for plots T-C, S-A and S-E (Fig. 5). According to the two-resistance exchange interface model, the exchange fluxes of Hg are controlled by the gradient of TGM concentrations at both interfaces (Zhang et al., 2002). As a result elevated atmospheric TGM concentrations should decrease the diffusion of soil pore TGM to the atmosphere. In a companion study, the soil pore TGM concentrations were measured at all the plots at the subtropical and temperate forests, except the wetlands (Zhou et al., in review). These results showed that gradient of TGM concentrations between the surface air and pore air at 3 cm were significantly correlated with the soil-air TGM fluxes at all the plots (Fig. S11 and S12). These results are

consistent with an experiment conducted at this subtropical forest, where artificially increasing ambient-air TGM concentrations significantly inhibited soil Hg volatilization (Zhou et al., 2017b). SEM inferred that that air TGM concentrations was the second important driver influencing the soil-air TGM exchange in Masson pine (Plot S-B), evergreen broad-leaved and wetland plots at subtropical forest (Fig. 5).

Xin and Gustin (2007) and Gustin et al. (2006) defined an associated concept of the compensation point for soils, which is the atmospheric Hg concentration at which the net Hg flux between the soil and the atmosphere was zero. If the atmospheric TGM concentration is above compensation point, atmospheric deposition occurs; if the concentration is below the compensation point soil emission occurs. A strong linear relationships are shown in Figs. 5 and 6 ($p < 0.01$), resulting in compensation points of 2.47, 2.97, 6.00, 3.33 and 3.50 ng m^{-3} for Chinese pine, larch, wetland, mixed broad-leaved forests and open field at the temperate forest with area-weighted compensation point of 3.42 ng m^{-3}. The compensation points were much higher at the subtropical forest, with values of 6.50, 7.71, 3.92, 3.83 and 12.91 ng m^{-3} for Masson pine upland and mid-slope, wetland, broad-leaved and open field at the subtropical forest with area-weighted compensation point of 6.82 ng m^{-3}. Another study of subtropical coniferous forest showed similar compensation point (7.75 ng m^{-3}) as those in the Masson pine forests of our study (Luo, 2015).

Diurnal variation in soil-air TGM fluxes were measured in plot S-A at the subtropical forest (Fig. 8) and in plot T-D at the temperate forest (Fig. 9). Soil TGM fluxes were well correlated with soil and air temperature ($p < 0.01$ for all) and were highly dependent on solar radiation in spring, summer and autumn ($p < 0.01$ for all) but not in winter ($p > 0.05$), which are similar to seasonal patterns from other studies (Howard and Edwards, 2018;Osterwalder et al., 2018;Johnson et al., 2003). Solar radiation has been shown to promote photochemical reduction of soil-bound Hg and enrich Hg(0) in soil pore gas. This reaction is kinetically enhanced at higher temperatures (Eckley et al., 2015;Lin et al., 2010;Zhang et al., 2001). Compared to the other three seasons, the relatively low soil temperature (5.95 °C at the subtropical forest and –5.66 °C at the temperate forest) may have limited the relationship between soil TGM flux and solar radiation during the winter season.

4. Conclusions and study implications

Prior to undertaking these measurements of Hg air-surface exchange flux, no direct

measurement of Hg exchange flux were available for background landscapes in North China. Our detailed direct observations have important implications for the role of forests in global and regional Hg cycles. Through multi-plot measurements over 130 and 96 days at the subtropical and temperate forests in China, we were able to reduce the uncertainty of soil-atmosphere TGM fluxes at the catchment scale and improve understanding of how landscape attributes contribute to variability in soil Hg evasion. It is inferred that forest soils acts as net TGM sources to the atmosphere. Strong correlations were evident between the soil Hg flux and environmental variables in some plots, such as solar radiation, temperature, soil moisture and air TGM concentrations.

The compensation points were determined for background forest soils from full-scale field data showing area-weighted values of 6.82 and 3.42 ng m^{-3} for the entire subtropical and temperate catchments, respectively. The values of compensation indicate that the atmospheric TGM concentration can play a critical role in limiting TGM fluxes between forest floor and atmosphere. Future studies need to focus on forest soils as an important increasing source of Hg to the atmosphere, because of recent declines in anthropogenic Hg emissions and TGM concentrations (Liu et al., 2019). Moreover TGM re-emissions are partially derived from legacy Hg stored in surface soils. A recent study using models simulating the dynamics of the subtropical forest landscape under climate change, harvesting, and land-use disturbances in southern China showed that coniferous forest area increased approximately 3.7 times compared to broad-leaved forest area (Wu et al., 2019). In the temperate forest, climatic changes in the northern China are expected to cause coniferous stands to transition to deciduous forests over the next hundred years (Ma et al., 2014). Climate change and land-use disturbance may increase the compensation points in both temperate and subtropical forests, therefore, increasing emissions of legacy Hg from terrestrial soils to the atmosphere. Some studies have emphasized that climate and land use change will potentially enhance deposition of Hg to forested landscapes (Haynes et al., 2017;Richardson and Friedland, 2015;Li et al., 2020); however, our study suggests that legacy Hg in forest soils could be emitted back to atmosphere, offsetting enhanced atmospheric Hg deposition. Better understanding of the response of Hg emissions from forest soils to climate and land use change is an important topic for future research.

Data availability. The data will be available upon request to the corresponding author.

References:

Agnan, Y., Le, D. T., Moore, C., Edwards, G., and Obrist, D.: New constraints on terrestrial surface-atmosphere fluxes of gaseous elemental mercury using a global database, Environmental Science & Technology, 50, 507−524, 10.1021/acs.est.5b04013, 2016.

Angot, H., Dastoor, A., De Simone, F., Gardfeldt, K., Gencarelli, C. N., Hedgecock, I. M., Langer, S., Magand, O., Mastromonaco, M. N., Nordstrom, C., Pfaffhuber, K. A., Pirrone, N., Ryjkov, A., Selin, N. E., Skov, H., Song, S., Sprovieri, F., Steffen, A., Toyota, K., Travnikov, O., Yang, X., and Dommergue, A.: Chemical cycling and deposition of atmospheric mercury in polar regions: review of recent measurements and comparison with models, Atmospheric Chemistry and Physics, 16, 10735-10763, 10.5194/acp-16-10735-2016, 2016.

Breuer, L., Kiese, R., and Butterbachbahl, K.: Temperature and moisture effects on nitrification rates in tropical rain-forest soils, Soil Science Society of America Journal, 66, 399-402, 2002.

Carpi, A., Fostier, A. H., Orta, O. R., dos Santos, J. C., and Gittings, M.: Gaseous mercury emissions from soil following forest loss and land use changes: Field experiments in the United States and Brazil, Atmospheric Environment, 96, 423-429, 10.1016/j.atmosenv.2014.08.004, 2014.

Chen, Y., Yin, Y., Shi, J., Liu, G., Hu, L., Liu, J., Cai, Y., and Jiang, G.: Analytical methods, formation, and dissolution of cinnabar and its impact on environmental cycle of mercury, Critical Reviews in Environmental Science and Technology, 47, 2415-2447, 10.1080/10643389.2018.1429764, 2017.

Cheng, Z., Tang, Y., Li, E., Wu, Q., Wang, L., Liu, K., Wang, S., Huang, Y., and Duan, L.: Mercury accumulation in soil from atmospheric deposition in temperate steppe of Inner Mongolia, China, Environmental Pollution, 258, 10.1016/j.envpol.2019.113692, 2020.

Choi, H.-D., and Holsen, T. M.: Gaseous mercury emissions from unsterilized and sterilized soils: The effect of temperature and UV radiation, Environmental Pollution, 157, 1673-1678, 10.1016/j.envpol.2008.12.014, 2009a.

Choi, H. D., and Holsen, T. M.: Gaseous mercury fluxes from the forest floor of the Adirondacks,

775   Environmental Pollution, 157, 592-600, 2009b.

776   Du, B., Zhou, J., Zhou, L., Fan, X., and Zhou, J.: Mercury distribution in the foliage and soil profiles of

777   a subtropical forest: Process for mercury retention in soils, Journal of Geochemical Exploration, 205,

778   10.1016/j.gexplo.2019.106337, 2019.

779   Durnford, D., and Dastoor, A.: The behavior of mercury in the cryosphere: A review of what we know

780   from observations, Journal of Geophysical Research: Atmospheres, 116, 10.1029/2010jd014809,

781   2011.

782   Eckley, C. S., Gustin, M., Lin, C. J., Li, X., and Miller, M. B.: The influence of dynamic chamber design

783   and operating parameters on calculated surface-to-air mercury fluxes, Atmospheric Environment, 44,

784   194-203, 10.1016/j.atmosenv.2009.10.013, 2010.

785   Eckley, C. S., Blanchard, P., Mclennan, D., Mintz, R., and Sekela, M.: Soil–air mercury flux near a large

786   industrial emission source before and after closure (Flin Flon, Manitoba, Canada), Environmental

787   Science & Technology, 49, 9750-9757, 2015.

788   Fang, J., Liu, G., Zhu, B., Wang, X., and Liu, S.: Carbon budgets of three temperate forest ecosystems

789   in Dongling Mt., Beijing, China, Science in China Series D-Earth Sciences, 50, 92-101,

790   10.1007/s11430-007-2031-3, 2007.

791   FAO: UNESCO soil map of the world, revised legend, in, World Res. Rep., 138, 1988.

792   Fraser, A., Dastoor, A., and Ryjkov, A.: How important is biomass burning in Canada to mercury

793   contamination?, Atmospheric Chemistry and Physics, 18, 7263-7286, 10.5194/acp-18-7263-2018,

794   2018.

795   Fu, X., Feng, X., and Wang, S.: Exchange fluxes of Hg between surfaces and atmosphere in the eastern

796   flank of Mount Gongga, Sichuan province, southwestern China, Journal of Geophysical Research-

797   Atmospheres, 113, 253-270, 2008.

798   Gao, Y., Wang, Z., Zhang, X., and Wang, C.: Observation and estimation of mercury exchange fluxes

799   from soil under different crop cultivars and planting densities in North China Plain, Environmental

800   pollution, 259, 113833, 10.1016/j.envpol.2019.113833, 2020.

801   Gustin, M. S.: Are mercury emissions from geologic sources significant? A status report, Science of the

802   Total Environment, 304, 153, 2003.

803   Gustin, M. S., and Stamenkovic, J.: Effect of watering and soil moisture on mercury emissions from soils,

804   Biogeochemistry, 76, 215-232, 2005.

805   Gustin, M. S., Engle, M., Ericksen, J., Lyman, S., Stamenkovic, J., and Xin, M.: Mercury exchange

806   between the atmosphere and low mercury containing substrates, Applied Geochemistry, 21, 1913-

807   1923, 2006.

808   Hararuk, O., Obrist, D., and Luo, Y.: Modelling the sensitivity of soil mercury storage to climate-induced

809   changes in soil carbon pools, Biogeosciences, 10, 2393-2407, 2013.

810   Hartman, J. S., Weisberg, P. J., Pillai, R., Ericksen, J. A., Kuiken, T., Lindberg, S. E., Zhang, H., Rytuba,

811   J. J., and Gustin, M. S.: Application of a rule-based model to estimate mercury exchange for three

812   background biomes in the continental United States, Environmental Science & Technology, 43, 4989-

813   4994, 10.1021/es900075q, 2009.

814   Haynes, K. M., Kane, E. S., Potvin, L., Lilleskov, E. A., Kolka, R. K., and Mitchell, C. P. J.: Gaseous

815   mercury fluxes in peatlands and the potential influence of climate change, Atmospheric Environment,

816   154, 247-259, https://doi.org/10.1016/j.atmosenv.2017.01.049, 2017.

817   Hou, H. Y.: Vegetation Map of P.R. China(1:4, 000, 000), Beijing, 1982.

818   Howard, D., and Edwards, G. C.: Mercury fluxes over an Australian alpine grassland and observation of

nocturnal atmospheric mercury depletion events, Atmospheric Chemistry and Physics, 18, 129-142, 10.5194/acp-18-129-2018, 2018.

Johnson, D. W., Benesch, J. A., Gustin, M. S., Schorran, D. S., Lindberg, S. E., and Coleman, J. S.: Experimental evidence against diffusion control of Hg evasion from soils, Science of the Total Environment, 304, 175, 2003.

Kamp, J., Skov, H., Jensen, B., and Sorensen, L. L.: Fluxes of gaseous elemental mercury (GEM) in the High Arctic during atmospheric mercury depletion events (AMDEs), Atmospheric Chemistry and Physics, 18, 6923-6938, 10.5194/acp-18-6923-2018, 2018.

Kiese, R., and Butterbach-Bahl, K.: N2O and CO2 emissions from three different tropical forest sites in the wet tropics of Queensland, Australia, Soil Biology & Biochemistry, 34, 975-987, 2002.

Kocman, D., and Horvat, M.: A laboratory based experimental study of mercury emission from contaminated soils in the River Idrijca catchment, Atmospheric Chemistry and Physics, 10, 1417-1426, 2010.

Kumari, A., Kumar, B., Manzoor, S., and Kulshrestha, U.: Status of Atmospheric Mercury Research in South Asia: A Review, Aerosol and Air Quality Research, 15, 1092-1109, 10.4209/aaqr.2014.05.0098, 2015.

Kuss, J., Krueger, S., Ruickoldt, J., and Wlost, K.-P.: High-resolution measurements of elemental mercury in surface water for an improved quantitative understanding of the Baltic Sea as a source of atmospheric mercury, Atmospheric Chemistry and Physics, 18, 4361-4376, 10.5194/acp-18-4361-2018, 2018.

Li, F., Ma, C., and Zhang, P.: Mercury Deposition, Climate Change and Anthropogenic Activities: A Review, Frontiers in Earth Science, 8, 10.3389/feart.2020.00316, 2020.

Lin, C. J., Gustin, M. S., Singhasuk, P., Eckley, C., and Miller, M.: Empirical models for estimating mercury flux from soils, Environmental Science & Technology, 44, 8522-8528, 2010.

Lin, H., Tong, Y., Yin, X., Zhang, Q., Zhang, H., Zhang, H., Chen, L., Kang, S., Zhang, W., Schauer, J., de Foy, B., Bu, X., and Wang, X.: First measurement of atmospheric mercury species in Qomolangma Natural Nature Preserve, Tibetan Plateau, and evidence of transboundary pollutant invasion, Atmospheric Chemistry and Physics, 19, 1373-1391, 10.5194/acp-19-1373-2019, 2019.

Liu, K., Wu, Q., Wang, L., Wang, S., Liu, T., Ding, D., Tang, Y., Li, G., Tian, H., Duan, L., Wang, X., Fu, X., Feng, X., and Hao, J.: Measure-specific effectiveness of air pollution control on China's atmospheric mercury concentration and deposition during 2013-2017, Environmental Science & Technology, 53, 8938-8946, 10.1021/acs.est.9b02428, 2019.

Luo, Y.: Mercury input, output and transport in forest ecosystems in southern China, Doctor's dissertation, Tsinghua University, Beijing, China, , pp. 1–112 pp., 2015.

Ly Sy Phu, N., Zhang, L., Lin, D.-W., Lin, N.-H., and Sheu, G.-R.: Eight-year dry deposition of atmospheric mercury to a tropical high mountain background site downwind of the East Asian continent, Environmental Pollution, 255, 10.1016/j.envpol.2019.113128, 2019.

Ma, J., Hu, Y., Bu, R., Chang, Y., Deng, H., and Qin, Q.: Predicting Impacts of Climate Change on the Aboveground Carbon Sequestration Rate of a Temperate Forest in Northeastern China, Plos One, 9, 10.1371/journal.pone.0096157, 2014.

Ma, M., Wang, D., Sun, R., Shen, Y., and Huang, L.: Gaseous mercury emissions from subtropical forested and open field soils in a national nature reserve, southwest China, Atmospheric Environment, 64, 116-123, 2013.

Ma, M., Sun, T., Du, H., and Wang, D.: A Two-Year Study on Mercury Fluxes from the Soil under

863   Different Vegetation Cover in a Subtropical Region, South China, Atmosphere, 9,
864   10.3390/atmos9010030, 2018.

865 Manca, G., Ammoscato, I., Esposito, G., Ianniello, A., Nardino, M., and Sprovieri, F.: Dynamics of snow-
866   air mercury exchange at Ny Ålesund during springtime 2011, E3S Web of Conferences, 1, 03010,
867   2013.

868 Maxwell, J. A., Holsen, T. M., and Mondal, S.: Gaseous elemental mercury (GEM) emissions from snow
869   surfaces in northern New York, Plos One, 8, e69342, 2013.

870 Mo, F., Li, X., He, S., and Wang, X.: Evaluation of soil and water conservation capacity of different
871   forest types in Dongling Mountain, Shengtai Xuebao/Acta Ecologica Sinica, 31, 5009-5016, 2011.

872 Nagati, M., Roy, M., DesRochers, A., Bergeron, Y., and Gardes, M.: Importance of soil, stand, and
873   mycorrhizal fungi inabiesbalsameaestablishment in the boreal forest, Forests, 11, 10.3390/f11080815,
874   2020.

875 O'Connor, D., Hou, D., Ok, Y. S., Mulder, J., Duan, L., Wu, Q., Wang, S., Tack, F. M. G., and Rinklebe,
876   J.: Mercury speciation, transformation, and transportation in soils, atmospheric flux, and implications
877   for risk management: A critical review, Environment International, 126, 747-761,
878   10.1016/j.envint.2019.03.019, 2019.

879 Obrist, D., Faïn, X., and Berger, C.: Gaseous elemental mercury emissions and CO(2) respiration rates
880   in terrestrial soils under controlled aerobic and anaerobic laboratory conditions, Science of the Total
881   Environment, 408, 1691-1700, 2010.

882 Obrist, D.: Mercury distribution across 14 U.S. forests. Part II: Patterns of methyl mercury concentrations
883   and areal mass of total and methyl mercury, Environmental Science & Technology, 46, 7434, 2012.

884 Obrist, D., Pokharel, A. K., and Moore, C.: Vertical profile measurements of soil air suggest
885   immobilization of gaseous elemental mercury in mineral soil, Environmental Science & Technology,
886   48, 2242, 2014.

887 Obrist, D., Kirk, J. L., Zhang, L., Sunderland, E. M., Jiskra, M., and Selin, N. E.: A review of global
888   environmental mercury processes in response to human and natural perturbations: Changes of
889   emissions, climate, and land use, Ambio, 47, 116-140, 10.1007/s13280-017-1004-9, 2018.

890 Olson, C., Jiskra, M., Biester, H., Chow, J., and Obrist, D.: Mercury in Active-Layer Tundra Soils of
891   Alaska: Concentrations, Pools, Origins, and Spatial Distribution, Global Biogeochemical Cycles, 32,
892   1058-1073, 10.1029/2017gb005840, 2018.

893 Osterwalder, S., Sommar, J., Akerblom, S., Jocher, G., Fritsche, J., Nilsson, M. B., Bishop, K., and
894   Alewell, C.: Comparative study of elemental mercury flux measurement techniques over a
895   Fennoscandian boreal peatland, Atmospheric Environment, 172, 16-25,
896   10.1016/j.atmosenv.2017.10.025, 2018.

897 Osterwalder, S., Huang, J.-H., Shetaya, W. H., Agnan, Y., Frossard, A., Frey, B., Alewell, C., Kretzschmar,
898   R., Biester, H., and Obrist, D.: Mercury emission from industrially contaminated soils in relation to
899   chemical, microbial, and meteorological factors, Environmental Pollution, 250, 944-952,
900   10.1016/j.envpol.2019.03.093, 2019.

901 Outridge, P. M., Mason, R. P., Wang, F., Guerrero, S., and Heimburger-Boavida, L. E.: Updated global
902   and oceanic mercury budgets for the united nations global mercury assessment 2018, Environmental
903   Science & Technology, 52, 11466-11477, 10.1021/acs.est.8b01246, 2018.

904 Pan, L., Lin, C.-J., Carmichael, G. R., Streets, D. G., Tang, Y., Woo, J.-H., Shetty, S. K., Chu, H.-W., Ho,
905   T. C., Friedli, H. R., and Feng, X.: Study of atmospheric mercury budget in East Asia using STEM-
906   Hg modeling system, Science of the Total Environment, 408, 3277-3291,

907   10.1016/j.scitotenv.2010.04.039, 2010.

908 Pannu, R., Siciliano, S. D., and O'Driscoll, N. J.: Quantifying the effects of soil temperature, moisture

909   and sterilization on elemental mercury formation in boreal soils, Environmental Pollution, 193, 138,

910   2014.

911 Peleg, M., Tas, E., Matveev, V., Obrist, D., Moore, C. W., Gabay, M., and Luria, M.: Observational

912   evidence for involvement of nitrate radicals in nighttime oxidation of mercury, Environmental

913   Science & Technology, 49, 14008, 2015.

914 Perez-Rodriguez, M., Biester, H., Aboal, J. R., Toro, M., and Martinez Cortizas, A.: Thawing of snow

915   and ice caused extraordinary high and fast mercury fluxes to lake sediments in Antarctica,

916   Geochimica Et Cosmochimica Acta, 248, 109-122, 10.1016/j.gca.2019.01.009, 2019.

917 Richardson, J. B., and Friedland, A. J.: Mercury in coniferous and deciduous upland forests in northern

918   New England, USA: implications of climate change, Biogeosciences, 12, 6737-6749, 10.5194/bg-

919   12-6737-2015, 2015.

920 Risch, M. R., DeWild, J. F., Gay, D. A., Zhang, L., Boyer, E. W., and Krabbenhoft, D. P.: Atmospheric

921   mercury deposition to forests in the eastern USA, Environmental Pollution, 228, 8-18,

922   10.1016/j.envpol.2017.05.004, 2017.

923 Slemr, F., Weigelt, A., Ebinghaus, R., Bieser, J., Brenninkmeijer, C. A. M., Rauthe-Schoech, A., Hermann,

924   M., Martinsson, B. G., van Velthoven, P., Boenisch, H., Neumaier, M., Zahn, A., and Ziereis, H.:

925   Mercury distribution in the upper troposphere and lowermost stratosphere according to

926   measurements by the IAGOS-CARIBIC observatory: 2014-2016, Atmospheric Chemistry and

927   Physics, 18, 12329-12343, 10.5194/acp-18-12329-2018, 2018.

928 Sørbotten, L. E.: Hill slope unsaturated flowpaths and soil moisture variability in a forested catchment

929   in Southwest China, MD, Department of Plant and Environmental Sciences, University of Life

930   Sciences, 2011.

931 Spolaor, A., Barbaro, E., Cappelletti, D., Turetta, C., Mazzola, M., Giardi, F., Bjorkman, M. P., Lucchetta,

932   F., Dallo, F., Pfaffhuber, K. A., Angot, H., Dommergue, A., Maturilli, M., Saiz-Lopez, A., Barbante,

933   C., and Cairns, W. R. L.: Diurnal cycle of iodine, bromine, and mercury concentrations in Svalbard

934   surface snow, Atmospheric Chemistry and Physics, 19, 13325-13339, 10.5194/acp-19-13325-2019,

935   2019.

936 St Louis, V. L., Graydon, J. A., Lehnherr, I., Amos, H. M., Sunderland, E. M., St Pierre, K. A., Emmerton,

937   C. A., Sandilands, K., Tate, M., Steffen, A., and Humphreys, E. R.: Atmospheric Concentrations and

938   Wet/Dry Loadings of Mercury at the Remote Experimental Lakes Area, Northwestern Ontario,

939   Canada, Environmental Science & Technology, 53, 8017-8026, 10.1021/acs.est.9b01338, 2019.

940 Sun, T., Ma, M., Wang, X., Wang, Y., Du, H., Xiang, Y., Xu, Q., Xie, Q., and Wang, D.: Mercury transport,

941   transformation and mass balance on a perspective of hydrological processes in a subtropical forest of

942   China, Environmental Pollution, 254, 10.1016/j.envpol.2019.113065, 2019.

943 Teixeira, D. C., Lacerda, L. D., and Silva-Filho, E. V.: Foliar mercury content from tropical trees and its

944   correlation with physiological parameters in situ, Environmental Pollution, 242, 1050-1057,

945   10.1016/j.envpol.2018.07.120, 2018.

946 Wang, Q., Luo, Y., Du, B., Ye, Z., and Duan, L.: Influencing factors of mercury emission flux from forest

947   soil at tieshanping,chongqing, Environmental Science, 35, 1922-1927, 2014.

948 Wang, S., Feng, X., Qiu, G., Fu, X., and Wei, Z.: Characteristics of mercury exchange flux between soil

949   and air in the heavily air-polluted area, eastern Guizhou, China, Atmospheric Environment, 41, 5584-

950   5594, 2007.

Wang, X., Bao, Z., Lin, C.-J., Yuan, W., and Feng, X.: Assessment of global mercury deposition through litterfall, Environmental science & technology, 50, 8548-8557, 2016.

Wang, X., Lin, C.-J., Feng, X., Yuan, W., Fu, X., Zhang, H., Wu, Q., and Wang, S.: Assessment of regional mercury deposition and emission outflow in mainland China, Journal of Geophysical Research-Atmospheres, 123, 9868-9890, 10.1029/2018jd028350, 2018.

Wang, Z., Zhang, X., Xiao, J., Zhijia, C., and Yu, P.: Mercury fluxes and pools in three subtropical forested catchments, southwest China, Environmental Pollution, 157, 801-808, 10.1016/j.envpol.2008.11.018, 2009.

Wang, Z. H., Zhang, G., Wang, Y., Zhao, Y. X., and Sun, X. J.: Research on mercury flux between snow and air under the condition of seasonal snow cover environment, Journal of Agro-Environment Science, 32, 601-606, 2013.

Wright, L. P., Zhang, L., and Marsik, F. J.: Overview of mercury dry deposition, litterfall, and throughfall studies, Atmospheric Chemistry and Physics, 16, 13399-13416, 10.5194/acp-16-13399-2016, 2016.

Wu, Z., Dai, E., Wu, Z., and Lin, M.: Future forest dynamics under climate change, land use change, and harvest in subtropical forests in Southern China, Landscape Ecology, 34, 843-863, 10.1007/s10980-019-00809-8, 2019.

Xin, M., and Gustin, M. S.: Gaseous elemental mercury exchange with low mercury containing soils: Investigation of controlling factors, Applied Geochemistry, 22, 1451-1466, 2007.

Yu, Q., Luo, Y., Xu, G., Wu, Q., Wang, S., Hao, J., and Duan, L.: Subtropical forests act as mercury sinks but as net sources of gaseous elemental mercury in south China, Environmental Science & Technology, 54, 2772-2779, 10.1021/acs.est.9b06715, 2020.

Yuan, W., Sommar, J., Lin, C.-J., Wang, X., Li, K., Liu, Y., Zhang, H., Lu, Z., Wu, C., and Feng, X.: Stable Isotope Evidence Shows Re-emission of Elemental Mercury Vapor Occurring after Reductive Loss from Foliage, Environmental Science & Technology, 53, 651-660, 10.1021/acs.est.8b04865, 2019a.

Yuan, W., Wang, X., Lin, C.-J., Sommar, J., Lu, Z., and Feng, X.: Process factors driving dynamic exchange of elemental mercury vapor over soil in broadleaf forest ecosystems, Atmospheric Environment, 219, 10.1016/j.atmosenv.2019.117047, 2019b.

Zarate-Valdez, J. L., Zasoski, R. J., and Lauchli, A.: Short-term effects of moisture content on soil solution pH and soil Eh, Soil Science, 171, 423-431, 10.1097/01.ss.0000222887.13383.08, 2006.

Zhang, G., Wang, N., Ai, J.-C., Zhang, L., Yang, J., and Liu, Z.-Q.: Characteristics of mercury exchange flux between soil and atmosphere under the snow retention and snow melting control, Huan jing ke xue= Huanjing kexue, 34, 468-475, 2013.

Zhang, H., Lindberg, S. E., Marsik, F. J., and Keeler, G. J.: Mercury air/surface exchange kinetics of background soils of the tahquamenon river watershed in the Michigan Upper Peninsula, Water Air & Soil Pollution, 126, 151-169, 2001.

Zhang, H., Lindberg, S. E., Barnett, M. O., Vette, A. F., and Gustin, M. S.: Dynamic flux chamber measurement of gaseous mercury emission fluxes over soils. Part 1: simulation of gaseous mercury emissions from soils using a two-resistance exchange interface model, Atmospheric Environment, 36, 835-846, 2002.

Zhang, H., Nizzetto, L., Feng, X., Borga, K., Sommar, J., Fu, X., Zhang, H., Zhang, G., and Larssen, T.: Assessing Air-Surface Exchange and Fate of Mercury in a Subtropical Forest Using a Novel Passive Exchange-Meter Device, Environmental Science & Technology, 53, 4869-4879, 10.1021/acs.est.8b06343, 2019a.

Zhang, L., Zhou, P., Cao, S., and Zhao, Y.: Atmospheric mercury deposition over the land surfaces and the associated uncertainties in observations and simulations: a critical review, Atmospheric Chemistry and Physics, 19, 15587-15608, 10.5194/acp-19-15587-2019, 2019b.

Zhang, Q., Huang, J., Wang, F., Mark, L., Xu, J., Armstrong, D., Li, C., Zhang, Y., and Kang, S.: Mercury distribution and deposition in glacier snow over western China, Environmental science & technology, 46, 5404, 2012.

Zhou, J., Wang, Z., Zhang, X., and Chen, J.: Distribution and elevated soil pools of mercury in an acidic subtropical forest of southwestern China, Environmental Pollution, 202, 187-195, 10.1016/j.envpol.2015.03.021, 2015.

Zhou, J., Wang, Z., Sun, T., Zhang, H., and Zhang, X.: Mercury in terrestrial forested systems with highly elevated mercury deposition in southwestern China: The risk to insects and potential release from wildfires, Environmental Pollution, 212, 188-196, 10.1016/j.envpol.2016.01.003, 2016.

Zhou, J., Wang, Z., Zhang, X., and Gao, Y.: Mercury concentrations and pools in four adjacent coniferous and deciduous upland forests in Beijing, China, Journal of Geophysical Research: Biogeosciences, 122, 1260-1274, 2017a.

Zhou, J., Wang, Z., Zhang, X., and Sun, T.: Investigation of factors affecting mercury emission from subtropical forest soil: A field controlled study in southwestern China, Journal of Geochemical Exploration, 176, 128-135, 10.1016/j.gexplo.2015.10.007, 2017b.

Zhou, J., Wang, Z., and Zhang, X.: Deposition and fate of mercury in litterfall, litter, and soil in coniferous and broad-leaved forests, Journal of Geophysical Research: Biogeosciences, 123, 2590-2603, 10.1029/2018jg004415, 2018.

Zhou, J., Du, B., Shang, L., Wang, Z., Cui, H., Fan, X., and Zhou, J.: Mercury fluxes, budgets, and pools in forest ecosystems of China: A review, Critical Reviews in Environmental Science and Technology, 50, 1411-1450, 2020.

Zhou, J., Wang, Z., Zhang, X., and Driscoll, C. T.: Measurement of vertical distribution of gaseous elemental mercury concentration in soil pore air at subtropical and temperate forests, in review.

Zhu, W., Lin, C. J., Wang, X., Sommar, J., Fu, X., and Feng, X.: Global observations and modeling of atmosphere-surface exchange of elemental mercury: a critical review, Atmospheric Chemistry & Physics, 16, 4451-4480, 2016.

1025 **Table 1.** Locations and summary of measurements (mean ± standard deviation) of soil-air TGM fluxes and environmental parameters at ten plots at the subtropical and
1026 temperate forests.

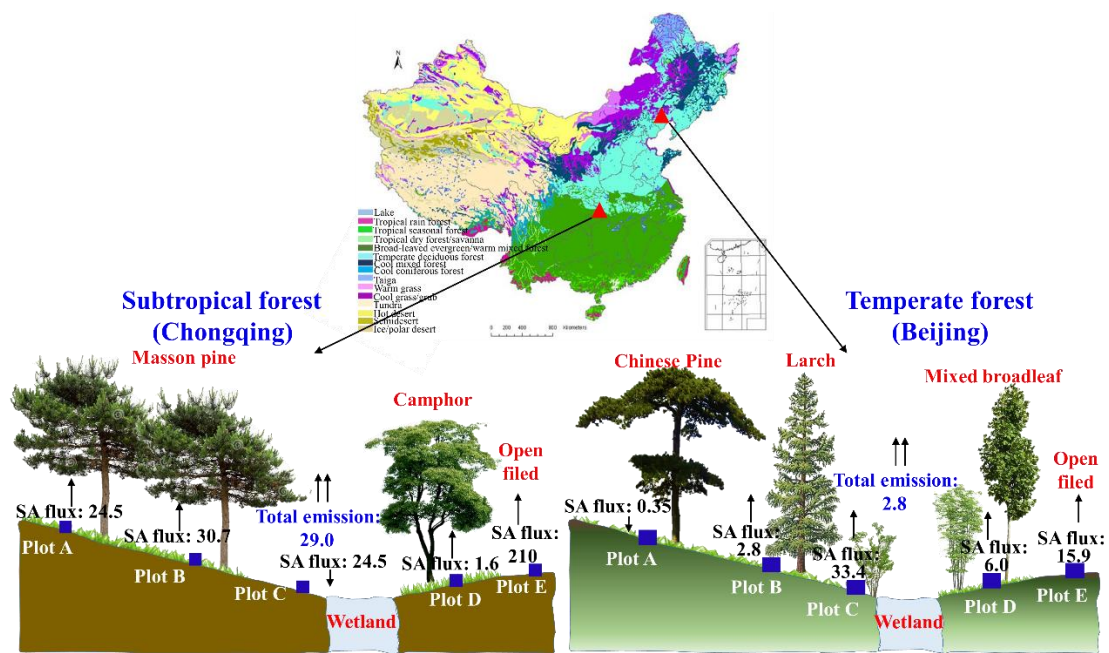| Forest	Plots	Locations	Flux (ng m^{-2} hr^{-1})	Soil surface TGM (ng m^{-3})	Soil Hg concentration (ng g^{-1})	SOM (0-5, %)	Soil moisture (%)	Soil temperature (°C)	Solar radiation (W m^{-2})
Subtropical forest	Plot S-A	Top-slope of coniferous forest	2.8 ± 3.9	3.6±1.3	219±15	13.6	0.3±0.1	16.8±7.6	39.9±27.5
	Plot S-B	Middle-slope of coniferous forest	3.5 ± 4.2	3.8±1.3	263±22	16.3	0.4±0.1	16.9±7.7	40.2±27.5
	Plot S-C	Wetland	-0.80 ± 5.1	3.7±1.4	96±43	4.9	0.3±0.1	16.7±7.5	30.5±27.9
	Plot S-D	Broad-leaved forest	0.18 ± 4.3	3.3±1.4	156±17	8.8	0.3±0.1	16.9±7.6	20.3±27.9
	Plot S-E	Open field	24 ± 33	4.1±1.7	159±18	4.1	0.3±0.1	18.3±8.5	98.0±138.4
Temperate forest	Plot T-A	Chinese pine forest	-0.04±0.81	2.22±0.87	72±12	5.8	17.0±8.55	9.77±6.57	17.09±29.4
	Plot T-B	Larch forest	0.32±0.96	2.30±0.94	141±15	25	26.3±6.51	10.0±6.23	22.9±18.6
	Plot T-C	Wetland	3.81±0.52	2.47±0.92	156±21	47	42.9±8.22	10.0±6.55	22.1±19.4
	Plot T-D	Mixed broad-leaved forest	0.68±1.01	2.37±0.87	74±9	16	25.4±7.32	9.86±6.26	25.9±18.6
	Plot T-E	Open field	1.82±0.79	1.98±0.79	52±4	12	27.9±5.56	10.1±6.47	47.1±29.4

1027

1028

1029 **Figure captions:**

1030 **Fig. 1.** Location of the five sampling plots and the estimation of soil-air fluxes (SA fluxes, values

1031   as g m^{-2} yr^{-1}) at the temperate and subtropical forest. Potential vegetation of China is from the

1032   Vegetation Map of China (Hou, 1982). Up and down arrows represent emission and deposition,

1033   respectively.

1034 **Fig. 2.** Mean and standard deviations of soil-air TGM fluxes at the five plots for the four seasons

1035   and annual values during the study at the subtropical forest (A) and temperate forest (B). The

1036   number of flux observations in spring, summer, autumn and winter were 62, 92, 66 and 43 at the

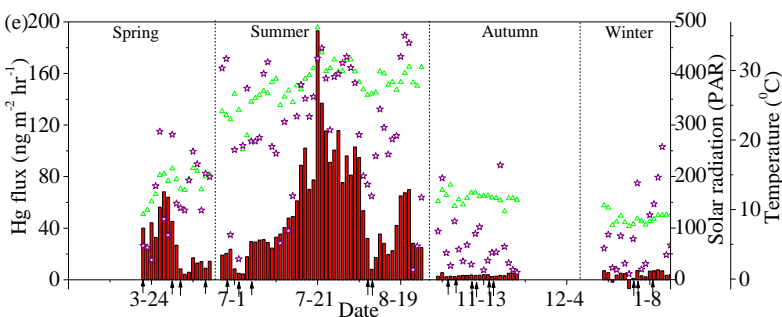1037   subtropical forest and 60, 58, 60 and 14 for the temperate forest, respectively.
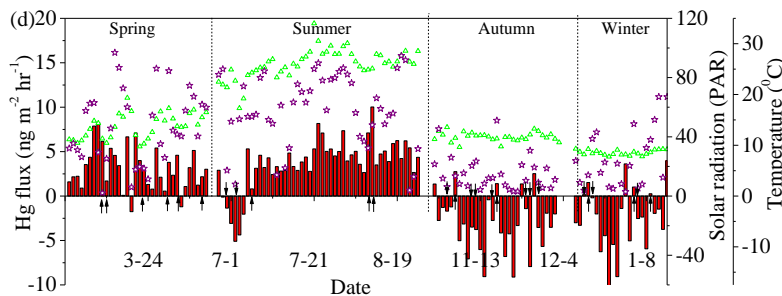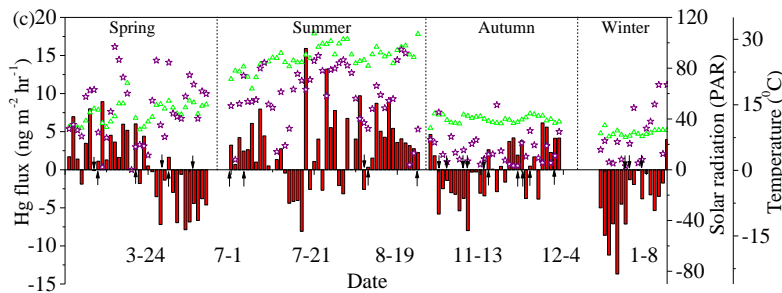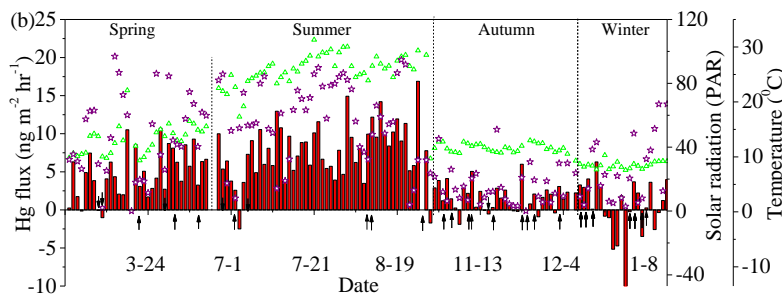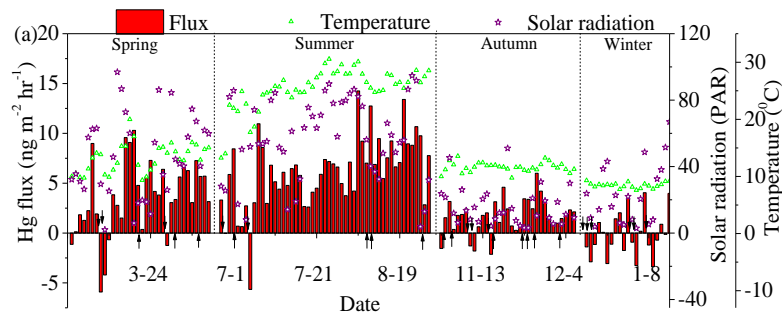
1038 **Fig. 3.** Daily (average flux of day and night) composite Hg flux, solar radiation and soil temperature

1039   at Masson pine forests plots ((A) and (B)), wetland (C), evergreen broad-leaved forest (D) and

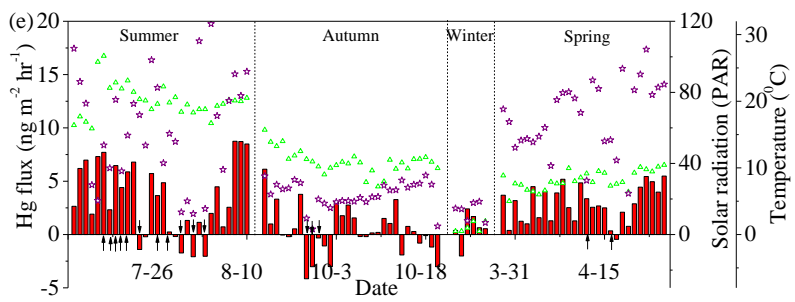1040   open field (E) plots at the subtropical forest. The vertical arrows represent precipitation events.
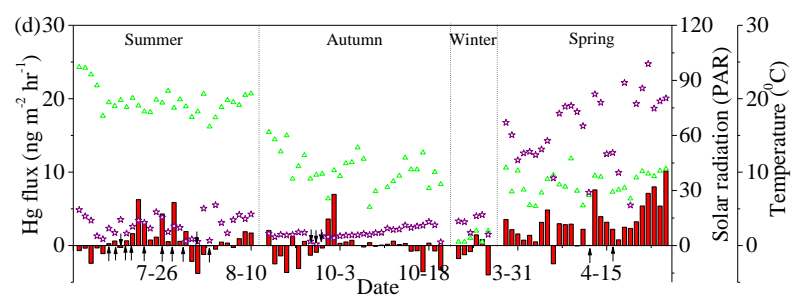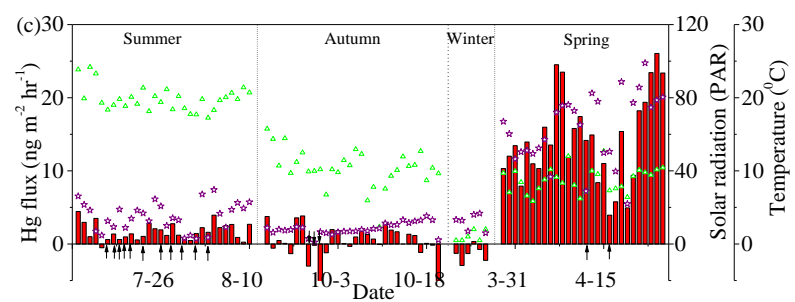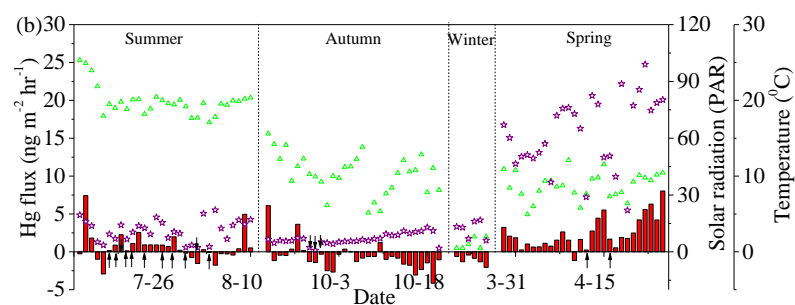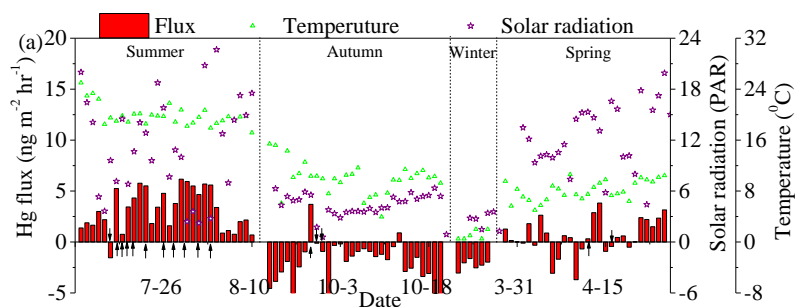
1041 **Fig. 4.** Daily (average flux of day and night) composite Hg flux, solar radiation and soil temperature

1042   at Chinese pine forest (A), larch forest (B), wetland (C), mixed broad-leaved forest (D) and open

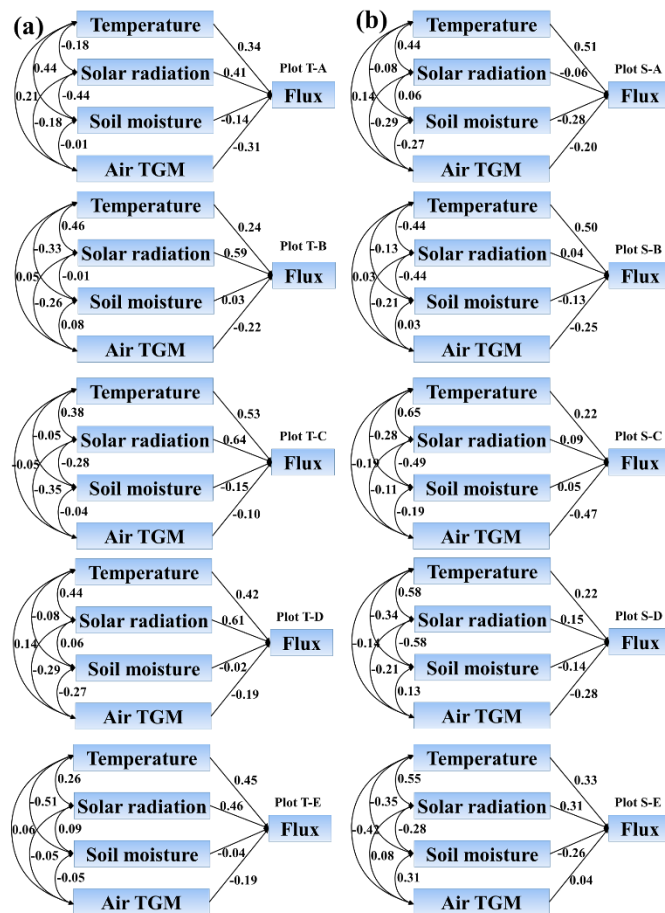1043   field (E) plots at the temperate forest. The vertical arrows represent precipitation events.

1044 **Fig. 5.** Interplays of environmental factors on air-soil TGM exchange flux obtained by structural

1045   equation model (SEM) in the temperate (a) and subtropical (b) forests.

1046 **Fig. 6.** Correlation between the air TGM concentration and air-surface Hg flux measured in daytime

1047   and night over four seasons for at Masson pine forest plots ((A) and (B)), wetland (C), evergreen

1048   broad-leaved forest (D) and open field (E) plots at the subtropical forest.

1049 **Fig. 7.** Correlation between the air TGM concentration and air-surface Hg flux measured in daytime

1050   and night over four seasons for the five plots at Chinese pine forest (a), larch forest (b), wetland

1051   (c), mixed broad-leaved forest (d) and open field (e) plots at the temperate forest.

1052 **Fig. 8.** Diurnal patterns of soil Hg fluxes with meteorological parameters in spring (a), summer (b),

1053   autumn (c) and winter (d) at the coniferous forest of the subtropical forest.

1054 **Fig. 9.** Diurnal patterns of soil Hg fluxes with meteorological parameters in spring (a), summer (b),

1055   autumn (c) and winter (d) at the deciduous broad-leaved forest of the temperate forest.

1056

1057

Fig. 1. Location of the five sampling plots and the estimation of soil-air fluxes (SA fluxes, values as g m^{-2} yr^{-1}) at the temperate and subtropical forest. Potential vegetation of China is from the Vegetation Map of China (Hou, 1982). Up and down arrows represent emission and deposition, respectively.
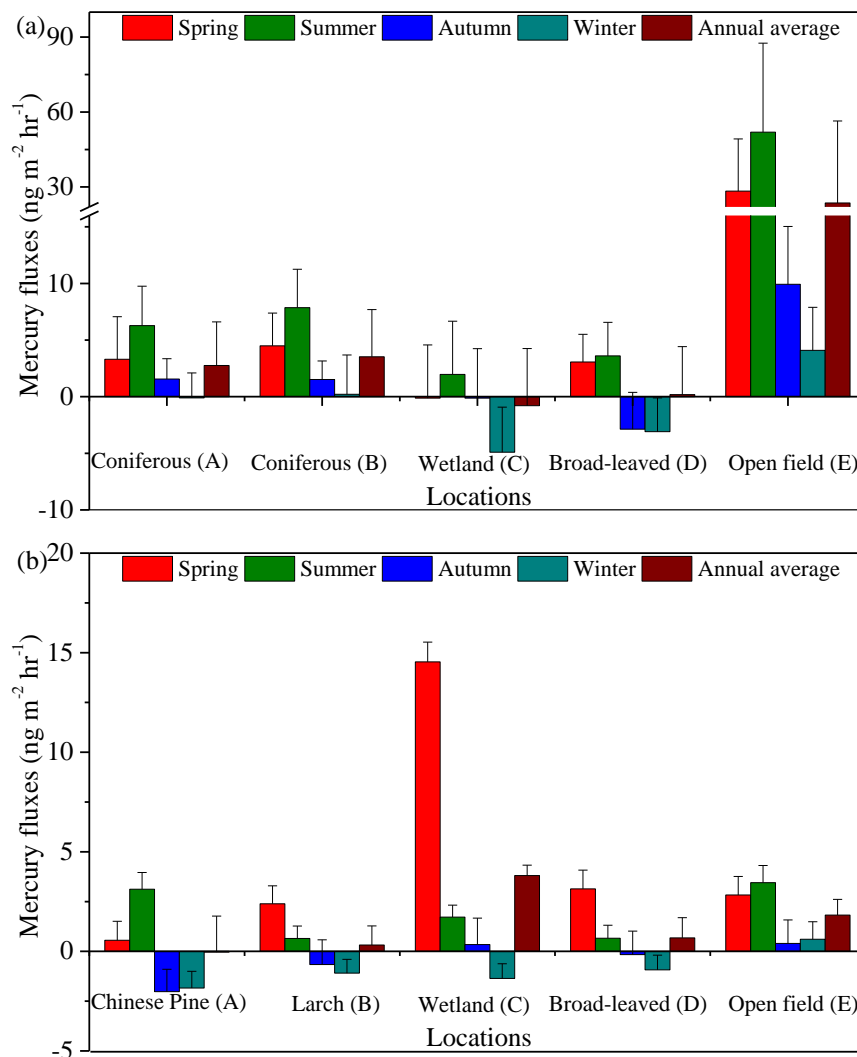
1058
1059
1060
1061
1062

1063

1064

1065 **Fig. 2.** Mean and standard deviations of soil-air TGM fluxes at the five plots for the four seasons
1066 and annual values during the study at the subtropical forest (A) and temperate forest (B). The
1067 number of flux observations in spring, summer, autumn and winter were 62, 92, 66 and 43 at the
1068 subtropical forest and 60, 58, 60 and 14 for the temperate forest, respectively.

1069

1070

1071

1072

1073

1074

Fig. 3. Daily (average flux of day and night) composite Hg flux, solar radiation and soil temperature at Masson pine forests plots ((A) and (B)), wetland (C), evergreen broad-leaved forest (D) and open field (E) plots at the subtropical forest. The vertical arrows represent precipitation events.
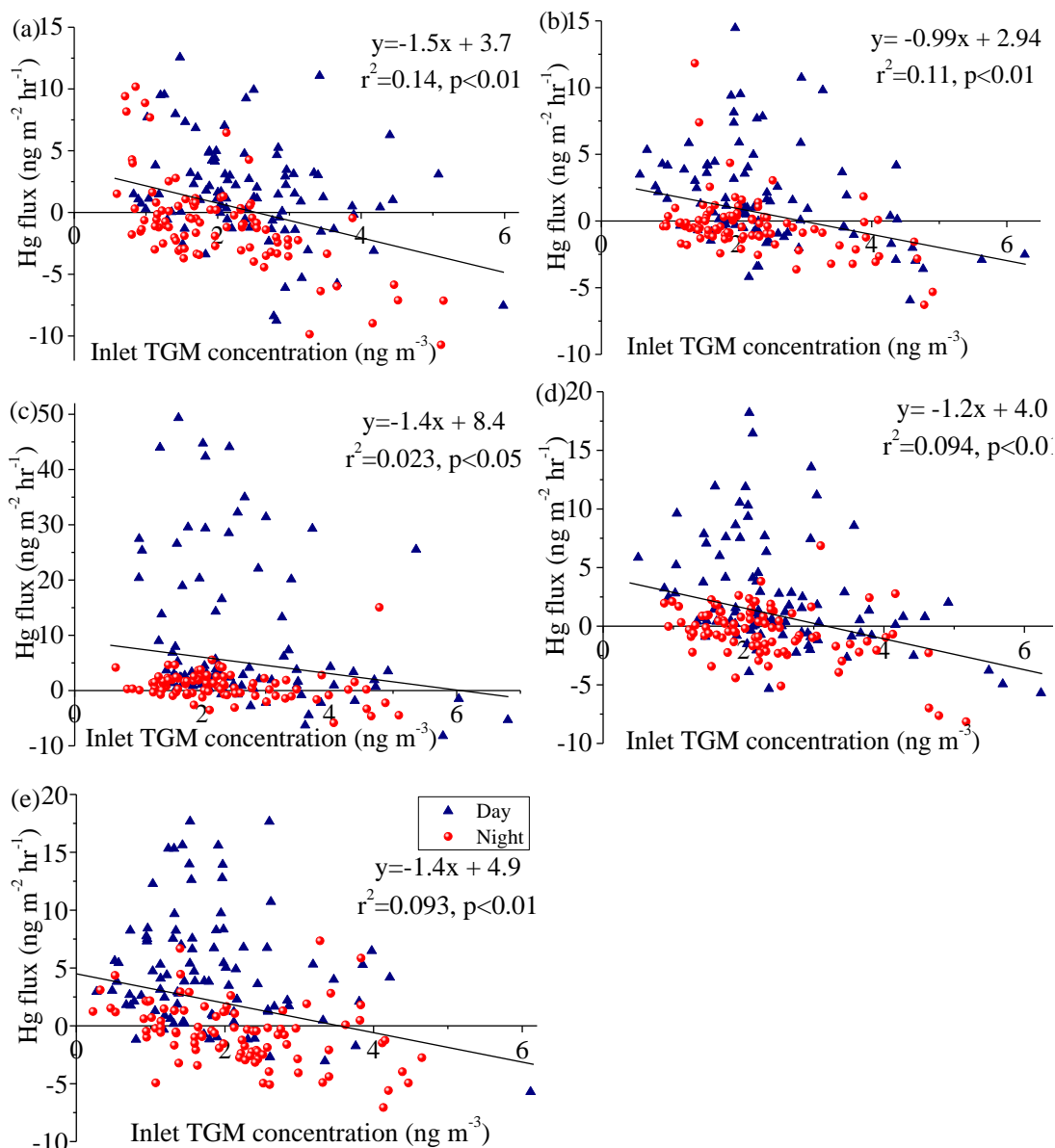
1075

1076

1077

1078

1079

1080

1081

1082

1083

Fig. 4. Daily (average flux of day and night) composite Hg flux, solar radiation and soil temperature
at Chinese pine forest (A), larch forest (B), wetland (C), mixed broad-leaved forest (D) and open
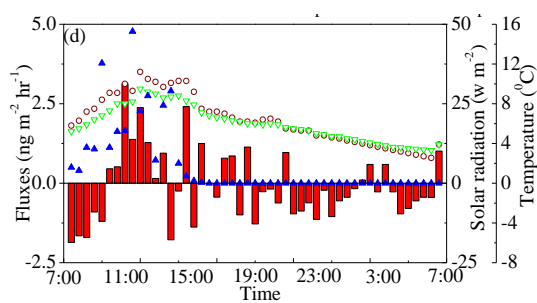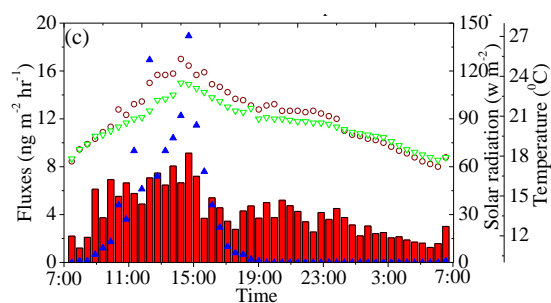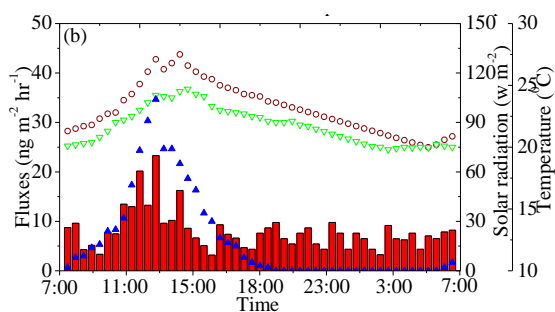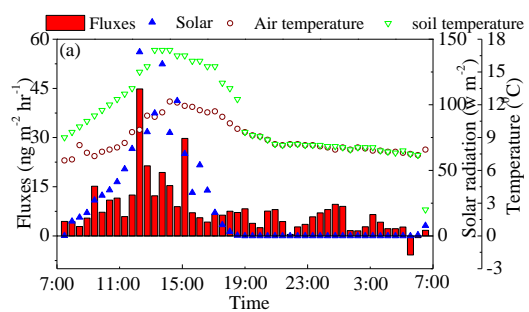field (E) plots at the temperate forest. The vertical arrows represent precipitation events.

1084
1085
1086
1087

1088

Fig. 5. Interplays of environmental factors on air-soil TGM exchange flux obtained by structural

1089

equation model (SEM) in the temperate (a) and subtropical (b) forests.

1090

1091

1092

1093

1094
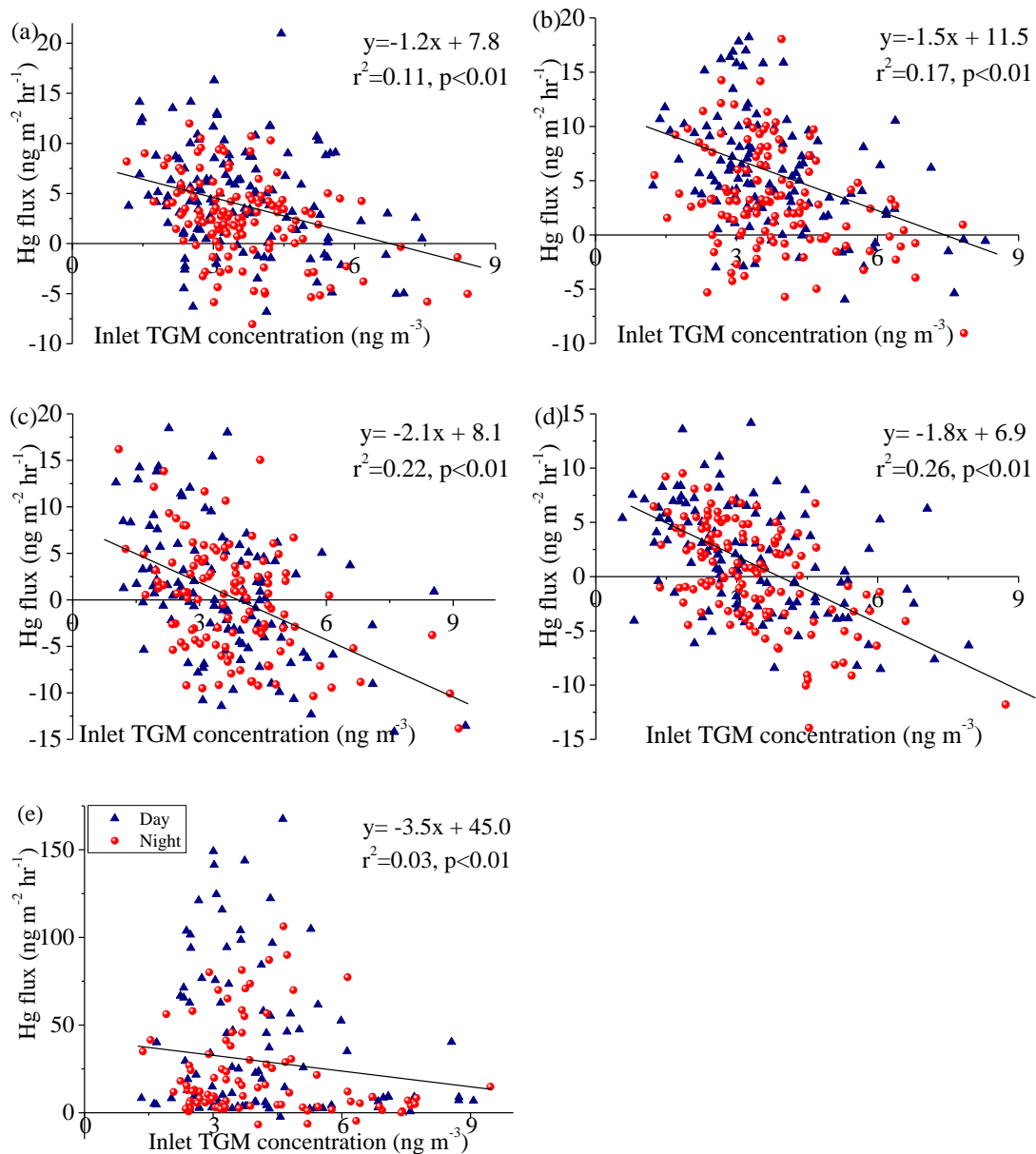
Fig. 6. Correlation between the air TGM concentration and air-surface Hg flux measured in daytime
and night over four seasons for at Masson pine forest plots ((A) and (B)), wetland (C), evergreen
broad-leaved forest (D) and open field (E) plots at the subtropical forest.

1095

1096

1097

1098

1099

1100

1101

1102 **Fig. 7.** Correlation between the air TGM concentration and air-surface Hg flux measured in daytime

1103 and night over four seasons for the five plots at Chinese pine forest (a), larch forest (b), wetland (c),

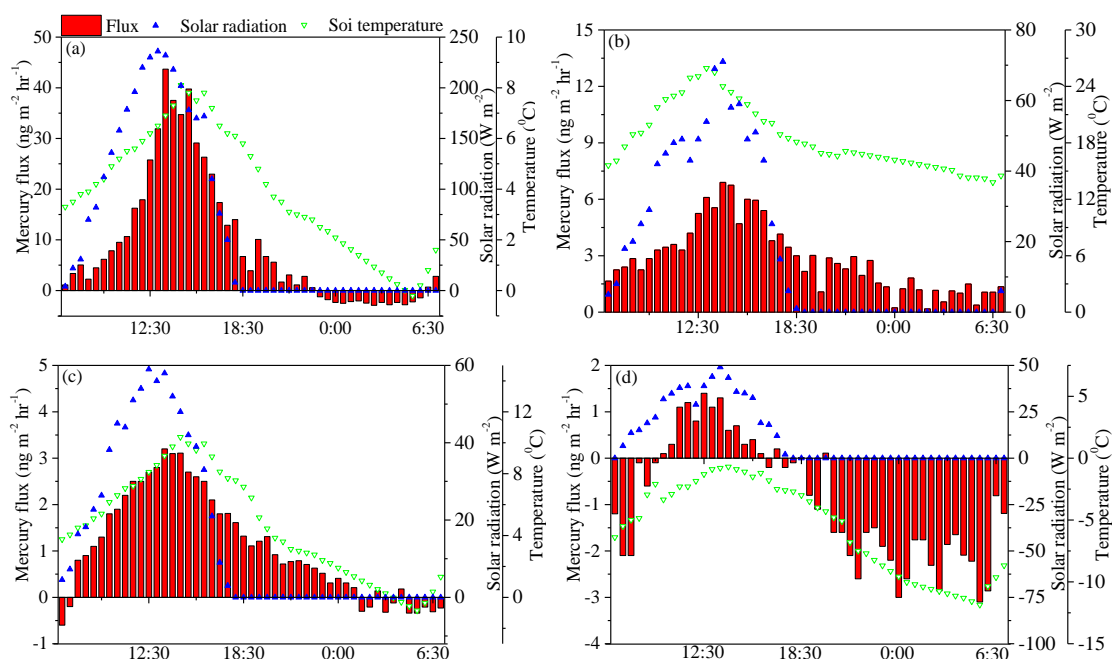1104 mixed broad-leaved forest (d) and open field (e) plots at the temperate forest.

1105

Fig. 8. Diurnal patterns of soil Hg fluxes with meteorological parameters in spring (a), summer (b), autumn (c) and winter (d) at the coniferous forest of the subtropical forest.

1106
1107
1108
1109
1110
1111

Fig. 9. Diurnal patterns of soil Hg fluxes with meteorological parameters in spring (a), summer (b), autumn (c) and winter (d) at the deciduous broad-leaved forest of the temperate forest.

Supporting Information

Soil-atmosphere exchange flux of total gaseous mercury (TGM) at subtropical and temperate forest catchments

Jun Zhou [a, b, c, f], Zhangwei Wang [a, c, *], Xiaoshan Zhang [a, c], Charles T. Driscoll [d], Che-Jen Lin [e]

a. State Key Laboratory of Urban and Regional Ecology, Research Center for Eco-Environmental Sciences, Chinese Academy of Sciences, Beijing 100085, China.

b. Key Laboratory of Soil Environment and Pollution Remediation, Institute of Soil Science, Chinese Academy of Sciences, Nanjing 210008, China.

c. University of Chinese Academy of Sciences, Beijing 100049, China.

d. Department of Civil and Environmental Engineering, Syracuse University, 151 Link Hall, Syracuse, New York 13244, United States.

e. Center for Advances in Water and Air Quality, Lamar University, Beaumont, Texas 77710, United States.

f. Department of Environmental, Earth and Atmospheric Sciences, University of Massachusetts, Lowell, 01854, USA

* Corresponding author: Zhangwei Wang

E-mail address: wangzhw@rcees.ac.cn (Z. Wang); Phone: +86 10 62849168.

No.18 Shuangqing Road, Beijing 100085, China

First author e-mail: zhoujun@issas.ac.cn (J. Zhou); Phone: +86 25 86881319.

No.73 East Beijing Road, Nanjing 210008, China.

Contents:

19 Pages

1 Tables

12 Figures

1147   *Supporting Text:*

1148   *Site description*

1149   In the subtropical forest, the mean annual precipitation, temperature and daily relative humidity

1150 at the TFP are 1230 mm, 18.2 °C and 95%, respectively. The ecosystem type at the TFP study site

1151 is a Masson Pine dominated forest, with some associated ever-green broad-leaved species. Trees

1152 were planted in the 1960s. The soil is typically mountain yellow earth (corresponding to a Haplic

1153 Acrisol in FAO). The soil is acidic, with a pH of 3.79. From previous studies, the mean Hg

1154 concentrations in precipitation, throughfall, litterfall and organic soils were 55.3 ng L^{-1}, 98.9 ng L^{-1},

1155 104.8±18.6 ng g^{-1} and 191 ± 65 ng g^{-1}, respectively, with an annual Hg input of 291.2 μg m^{-2} yr^{-1}

1156 (Zhou et al., 2016;Zhou et al., 2015).

1157   The temperate forest is located in the Xiaolongmen National Forest Park of Mt. Dongling near

1158 the Beijing Forest Ecosystem Research Station, Chinese Academy of Sciences (40°00′ N, 115°26′

1159 E), which is located 110 km southwest of Mega-city Beijing in North China. The elevation and is

1160 1300 m asl. The annual average rainfall is 612 mm and mean relative humidity is 66%. The Mt.

1161 Dongling is one of the Chinese Ecosystem Research Network (CERN) and Diversitas Western

1162 Pacific and Asia (DIWPA) monitoring sites. The region's climate is predominantly warm temperate

1163 continent monsoon climate with an annual average temperature 4.8 °C. Cool and dry climate in the

1164 study area has resulted in deep litter and high organic matter concentrations (Fang et al., 2007). The

1165 study area is a mature and secondary forest protected since the 1950s following the extensive

1166 deforestation. To characterize the terrestrial surface influence on the Hg fluxes, different ecosystems

1167 were selected to study the air-surface Hg fluxes from forest soil and snow at a sub-catchment (40

1168 ha) in the temperate forest, including the Chinese pine forest, larch forest, wetland, mixed broad-

1169 leaved forest and open field. The five sites were located about 200-300 m distance individually.

1170 From previous studies, the mean litterfall Hg concentrations were 15.8, 19.6, and 12.1 ng g^{-1} in

1171 Chinese pine forest, larch forest, and mixed broad-leaved forest plots and the mean soil Hg

1172 concentrations (0-5 cm) were 72±12, 141±15, and 74±9 ng g^{-1} in Chinese pine forest, larch forest,

1173 and mixed broad-leaved forest, respectively (Zhou et al., 2017).

1174

1175   *Environmental measurements*

1176   Daily meteorological parameters were collected and averaged over 5-min intervals. Daily air

1177 temperature and solar radiation were monitored using a TP 101 digital thermometer and a GLZ−C

1178 photo synthetically radiometer (TOP Ltd. China), respectively, during diurnal measurements. Soil

1179 percent moisture and soil temperature at 0-5 cm was monitored with Time Domain Reflectometry

1180 (TDR) Hydra Probe II (SDI−12/RS485) and a Stevens water cable tester (USA). Measurements

1181 were taken at the same time with gold trap collection. Solar radiation was collected with a weather

1182 station (Davis Wireless Vantage VUE 06250 Weather Station, Davis Instruments, Hayward, CA)

1183 located in the TFP Forest Station about 500 m away from the sub-catchment.

1184   For each DFC sampling location, bulk soil samples were collected from the DFC footprints

1185 (0−5 cm) in each month of study after the end of the measurement period. Soil samples were dried

1186 and homogenized, and completely ground to a fine powder in a pre-cleaned stainless-steel blender.

1187 The total Hg concentration in the soil samples was determined using a DMA-80 direct Hg analyzer

1188 (Milestone Ltd., Italy). SOM content in soils was determined using the sequential loss on ignition

1189 (LOI) method.(Zhou et al., 2013) A homogenized soil sample (WS) was dried at 105 °C for about

1190 12- 24 h to obtain the dry weight of the samples (DW_{105}). The heated dry sample was then

1191 combusted at 550 °C for 4 h and the weight of the sample after heating at 550 °C was DW_{550}. Thus,

1192 the TOM concentration (LOI_{550}) was calculated according to the following formula:

1193 $LOI_{550}=100(DW_{105}- DW_{550})/WS.$

1194 **Table S1.** Characteristics and detail of measurements at five plots in the forested sub-catchments.

Forest type	Plots	Locations	Date of flux measurement				Area (%)
			Spring	Summer	Autumn	Winter	
Subtropical forest	Plot S-A	Top-slope of coniferous forest	5 Mar-7 Apr	17 -19 Jun; 1-31 Jul; 10-24 Aug	3 Nov-6 Dec	24 Dec-14 Jan	42.4
	Plot S-B	Middle-slope of the coniferous forest	5 Mar-7 Apr	17 -19 Jun; 1-31 Jul; 10-24 Aug	3 Nov-6 Dec	24 Dec-14 Jan	42.4
	Plot S-C	Wetland	5 Mar-7 Apr	1-31 Jul; 10-24 Aug	3 Nov-6 Dec	31 Dec-14 Jan	2.9
	Plot S-D	Broad-leaved forest	5 Mar-7 Apr	17 -19 Jun; 1-31 Jul; 10-24 Aug	3 Nov-6 Dec	24 Dec-14 Jan	10
	Plot S-E	Open field	22 Mar-7 Apr	17 -19 Jun; 1-31 Jul; 10-24 Aug	3-23 Nov	30 Dec-14 Jan	2.3
Temperate forest	Plot T-A	Chinese pine forest	28 Mar–25 Apr	12 Jul–10 Aug	20 Sep–20 Oct	10–16 Nov	14
	Plot T-B	Larch forest	28 Mar–25 Apr	12 Jul–10 Aug	20 Sep–20 Oct	10–16 Nov	8
	Plot T-C	Wetland	28 Mar–25 Apr	12 Jul–10 Aug	20 Sep–20 Oct	10–16 Nov	9
	Plot T-D	Mixed broad-leaved forest	28 Mar–25 Apr	12 Jul–10 Aug	20 Sep–20 Oct	10–16 Nov	65
	Plot T-E	Open field	28 Mar–25 Apr	12 Jul–10 Aug	20 Sep–20 Oct	10–16 Nov	4

1195 Note: Area percent was according to Zhu et al. (2013) at the subtropical forest and Zhou et al. (1999) at the temperate forest.
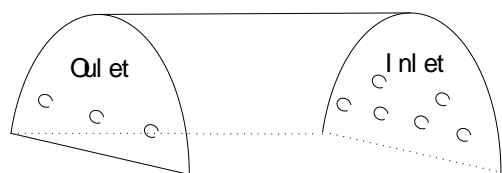
Figure Captions:

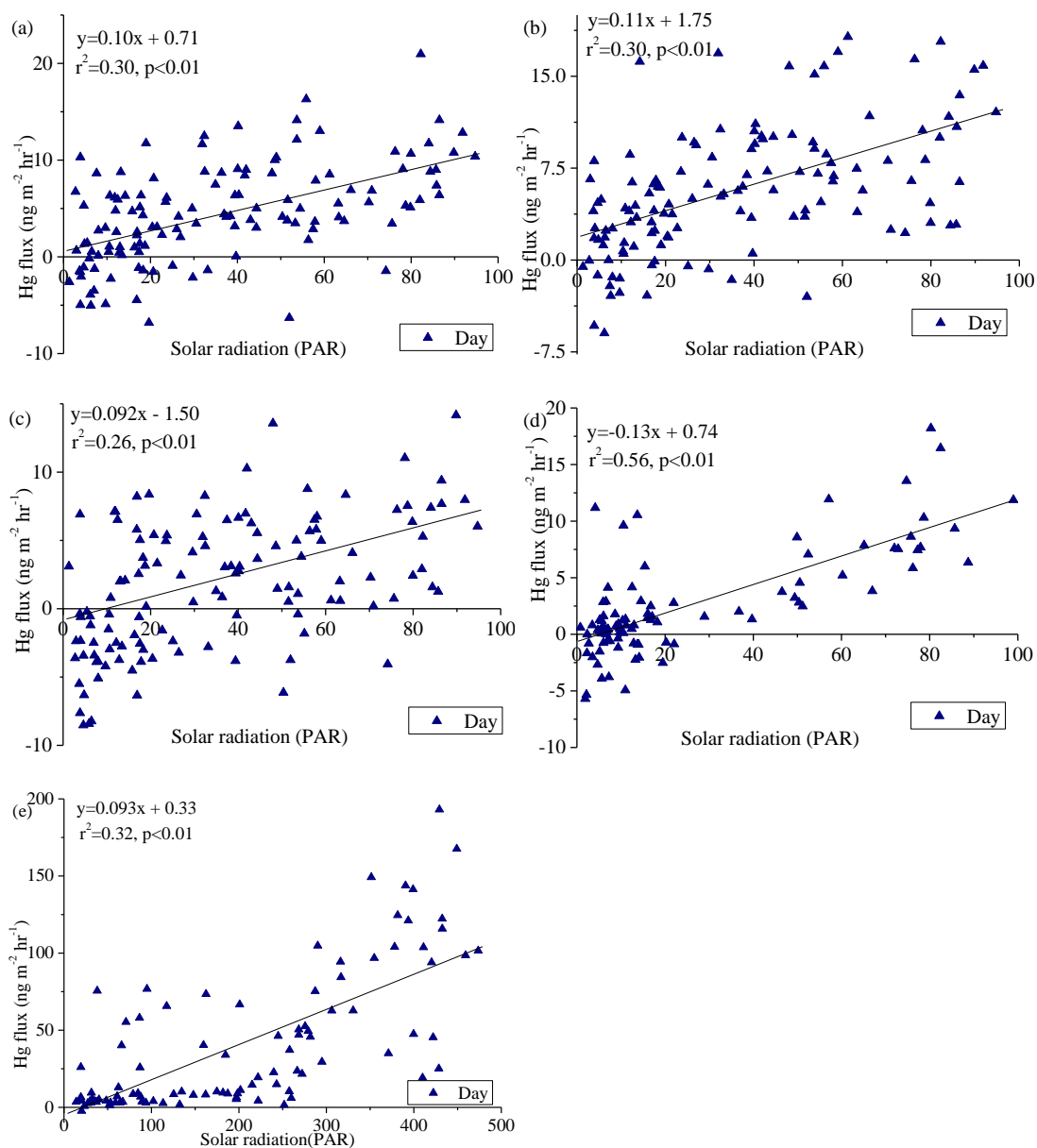**Fig. S1.** Schematic diagram of the dynamic flux chamber used in this study.

Fig. S2. Correlations between the averaged solar radiation (8:00-17:00) and air-surface Hg flux measured during daytime in Masson pine forests (a) and (b), wetland (c), evergreen broad-leaved forest (d) and open field (e) in the subtropical forest.

Fig. S3. Correlation between the averaged solar radiation (8:00-17:00) and air-surface Hg flux measured during daytime in Chinese pine forest (a), larch forest (b), wetland (c), mixed broad-leaved forest (d) and open field (e) in the temperate forest.

Fig. S4. Effects of rainfall events on annual soil-air TGM fluxes at Masson pine forests (Plot A) and (Plot B), wetland (Plot C), evergreen broad-leaved forest (Plot D) and open field (Plot E) at the subtropical forest (A), and at Chinese pine forest (Plot A), larch forest (Plot B), wetland (Plot C), mixed broad-leaved forest (Plot D) and open field (Plot E) at the temperate forest (B).

Fig. S5. Correlation between the soil Hg concentrations ($S_c \pm SD$) and soil-air Hg flux ($F \pm SD$) under the forest canopy at the subtropical forest. Standard deviations of soil Hg concentrations were obtained from Hg concentrations over the four seasons (n=12). Because fluxes are often controlled by solar radiation for bare soils, the correlation analysis above does not include data from the open field (plot E).

Fig. S6. Soil-air TGM fluxes during the daytime and nighttime at Masson pine forests (Plot A) and (Plot B), wetland (Plot C), evergreen broad-leaved forest (Plot D) and open field (Plot E) at the subtropical forest (a), and at Chinese pine forest (Plot A), larch forest (Plot B), wetland (Plot C), mixed broad-leaved forest (Plot D) and open field (Plot E) at the temperate forest (b).

Fig. S7. Correlations between soil temperature and air-surface Hg fluxes measured during daytime and night at the Masson pine forests (a) and (b), wetland (c), evergreen broad-leaved forest (d) and open field (e) in the subtropical forest.

Fig. S8. Correlations between soil temperature and air-surface Hg fluxes measured during daytime and night at the Chinese pine forest (a), larch forest (b), wetland (c), mixed broad-leaved forest (d) and open field (e) at the temperate forest.

1223 **Fig. S9.** Correlations between soil moisture and air-surface Hg fluxes measured during daytime and

1224 night at the Chinese pine forest (a), larch forest (b), wetland (c), mixed broad-leaved forest (d)

1225 and open field (e) at the subtropical forest.

1226 **Fig. S10.** Correlations between soil moisture and air-surface Hg fluxes measured during daytime

1227 and night at the Chinese pine forest (a), larch forest (b), wetland (c), mixed broad-leaved forest

1228 (d) and open field (e) at the temperate forest.

1229 **Fig. S11.** Correlations between the gradient of Hg(0) concentrations between surface soil pore (at 3

1230 cm) and atmospheric values and soil-air Hg(0) flux at four plots at the subtropical forest.

1231 **Fig. S12.** Correlations between the gradient of Hg(0) concentrations between surface soil pore (at 3

1232 cm) and atmospheric values and soil-air Hg(0) flux at the four plots at the temperate forest.

1233

1234

1235

1236   **Fig. S1.** Schematic diagram of the dynamic flux chamber used in this study.

1237

1238

1239

1240

1241

Fig. S2. Correlations between the averaged solar radiation (8:00-17:00) and air-surface Hg flux measured during daytime in Masson pine forests (a) and (b), wetland (c), evergreen broad-leaved forest (d) and open field (e) in the subtropical forest.
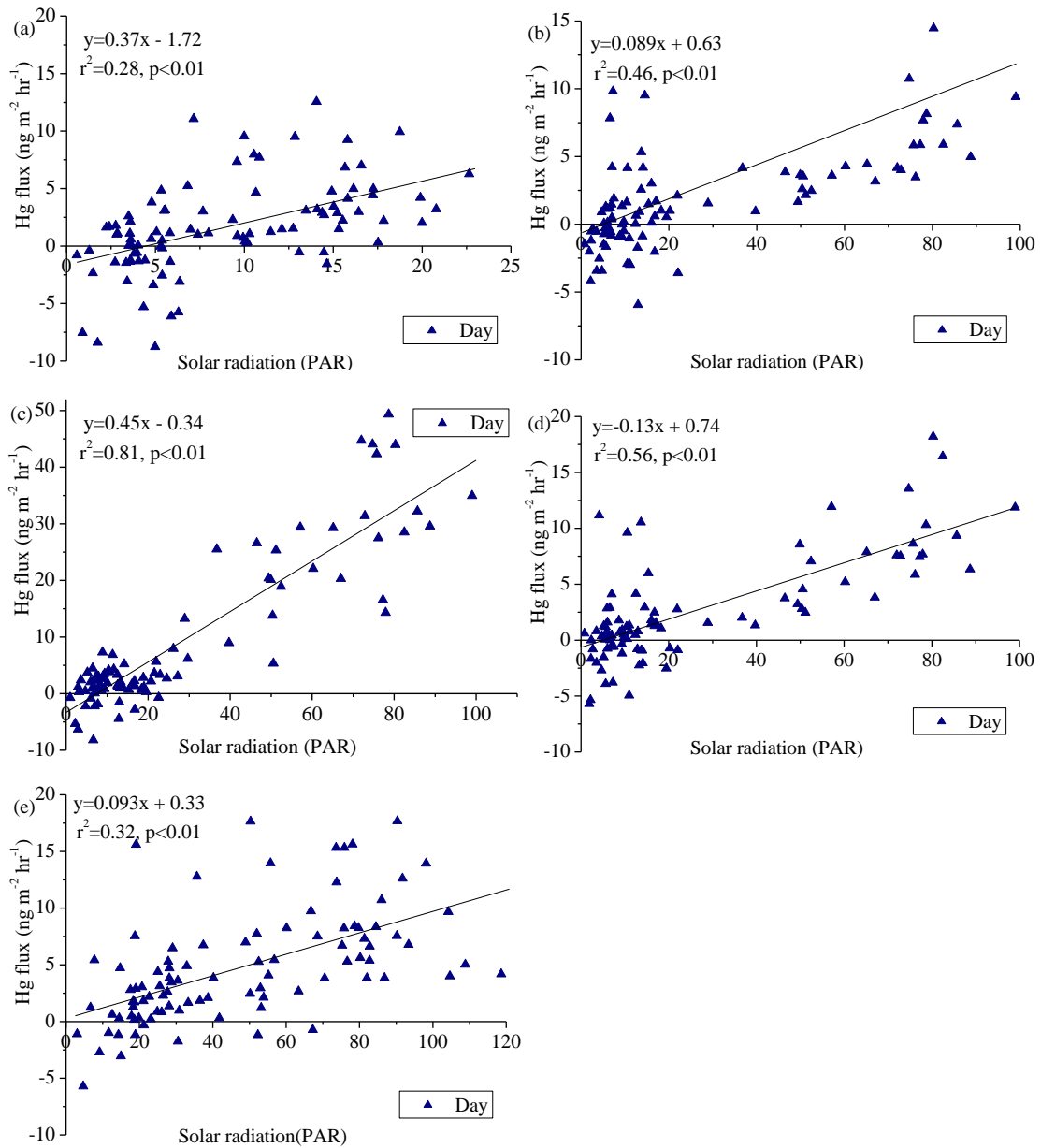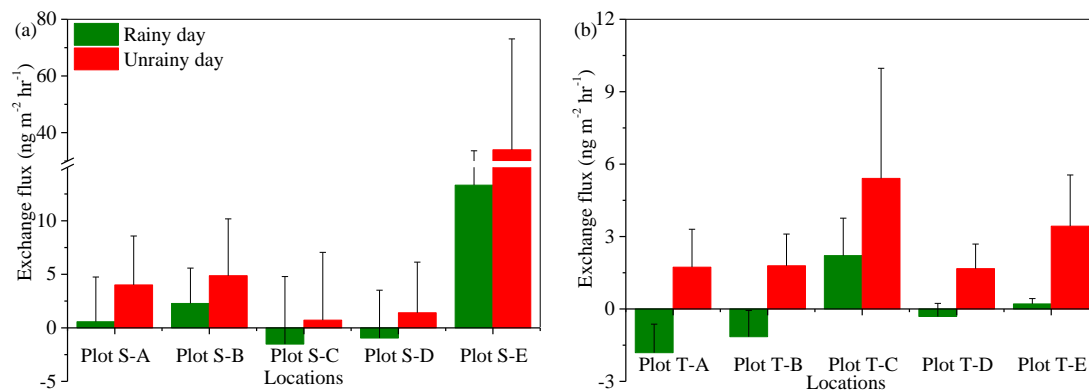
1242

1243

1244

1245

1246

1247

1248

1249 **Fig. S3.** Correlation between the averaged solar radiation (8:00-17:00) and air-surface Hg flux
1250 measured during daytime in Chinese pine forest (a), larch forest (b), wetland (c), mixed broad-
1251 leaved forest (d) and open field (e) in the temperate forest.

1252

1253

Fig. S4. Effects of rainfall events on annual soil-air TGM fluxes at Masson pine forests (Plot A) and (Plot B), wetland (Plot C), evergreen broad-leaved forest (Plot D) and open field (Plot E) at the subtropical forest (A), and at Chinese pine forest (Plot A), larch forest (Plot B), wetland (Plot C), mixed broad-leaved forest (Plot D) and open field (Plot E) at the temperate forest (B).
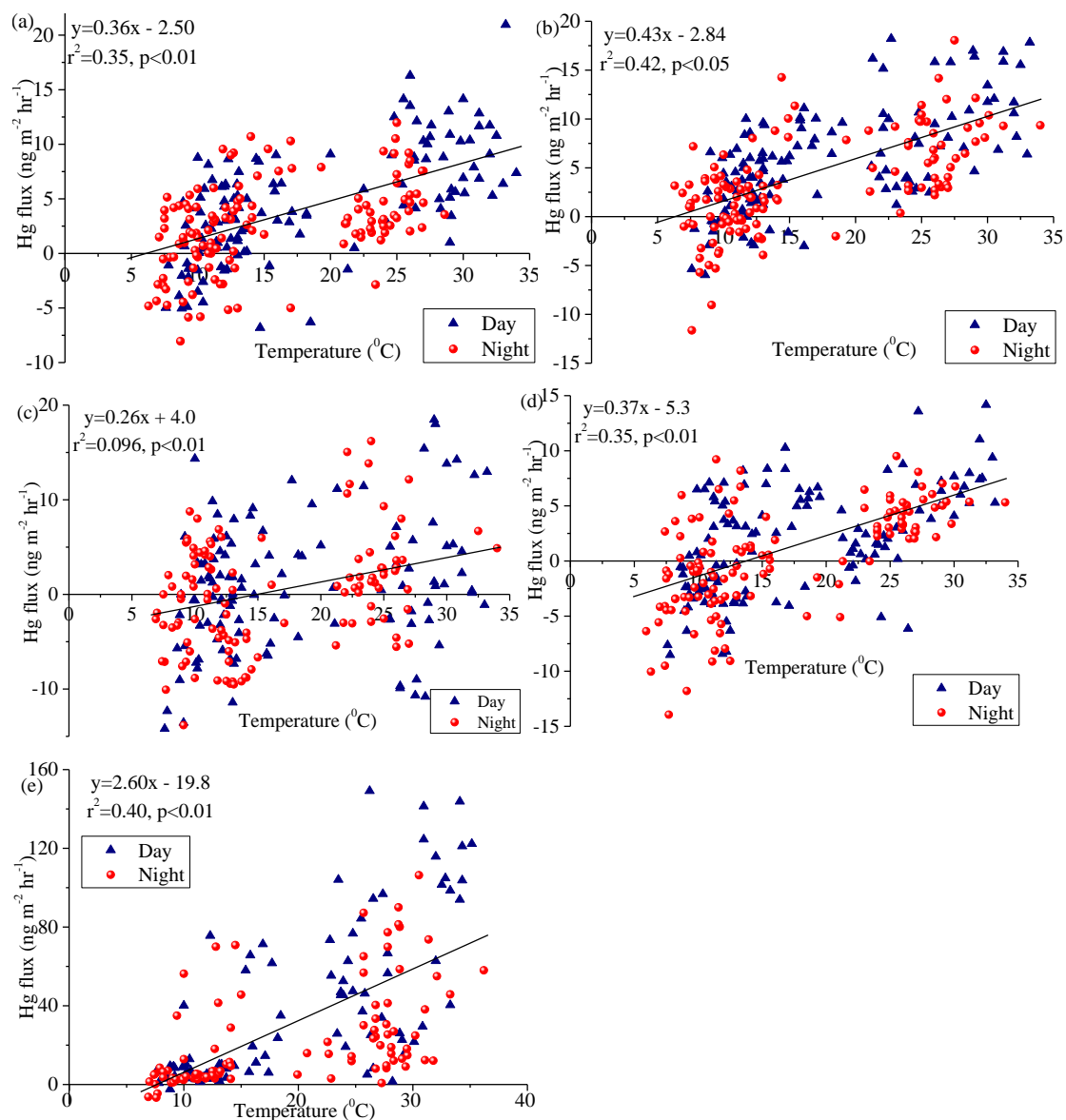
Fig. S5. Correlation between the soil Hg concentrations ($S_c \pm SD$) and soil-air Hg flux ($F \pm SD$) under the forest canopy at the subtropical forest. Standard deviations of soil Hg concentrations were obtained from Hg concentrations over the four seasons (n=12). Because fluxes are often controlled by solar radiation for bare soils, the correlation analysis above does not include data from the open field (plot E).

Fig. S6. Soil-air TGM fluxes during the daytime and nighttime at Masson pine forests (Plot A) and (Plot B), wetland (Plot C), evergreen broad-leaved forest (Plot D) and open field (Plot E) at the subtropical forest (a), and at Chinese pine forest (Plot A), larch forest (Plot B), wetland (Plot C), mixed broad-leaved forest (Plot D) and open field (Plot E) at the temperate forest (b).

1272

1273

1274

Fig. S7. Correlations between soil temperature and air-surface Hg fluxes measured during daytime
and night at the Masson pine forests (a) and (b), wetland (c), evergreen broad-leaved forest (d) and
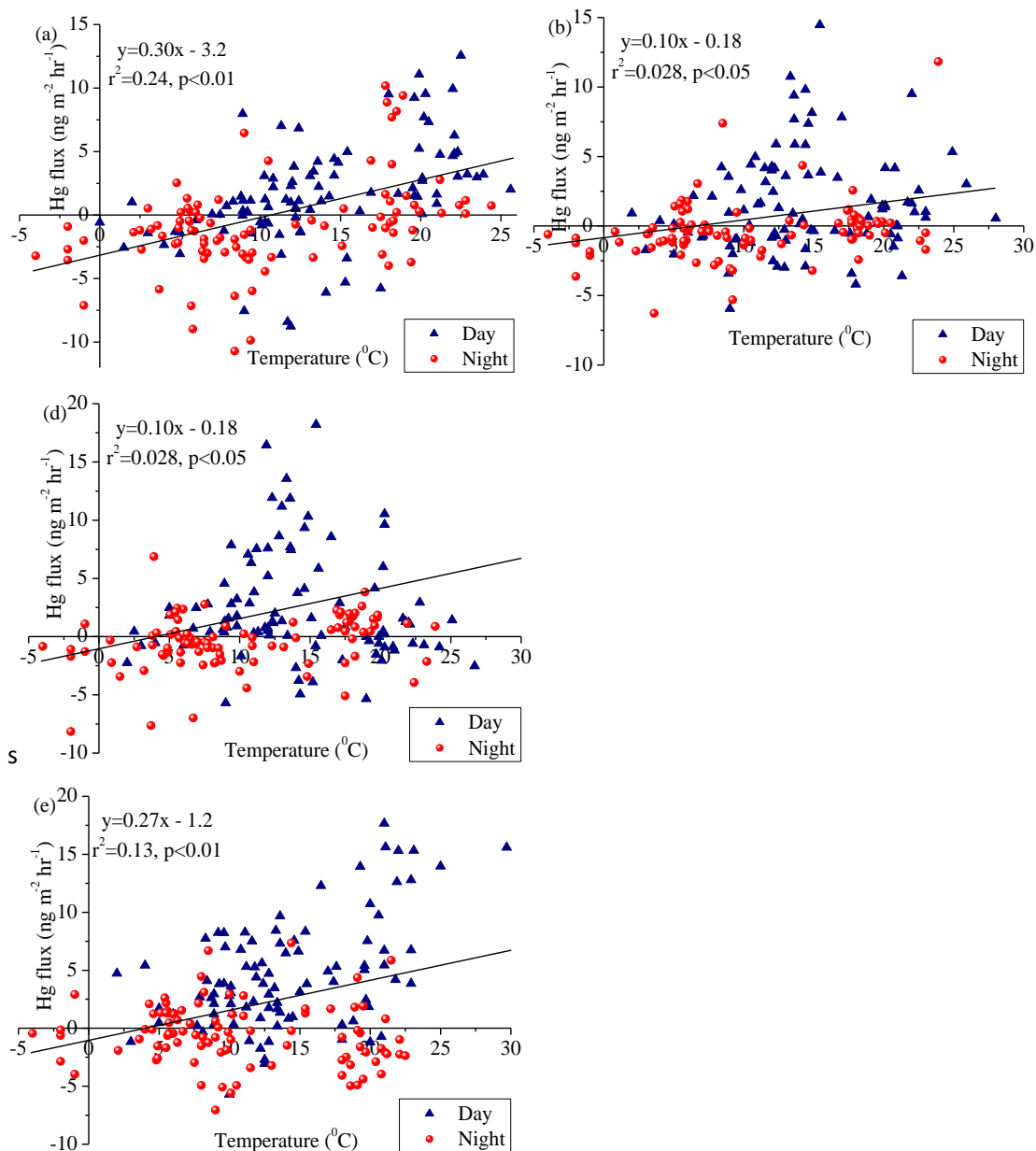open field (e) in the subtropical forest.

1275

1276

1277

1278

1279

1280   s

1281

Fig. S8. Correlations between soil temperature and air-surface Hg fluxes measured during daytime and night at the Chinese pine forest (a), larch forest (b), wetland (c), mixed broad-leaved forest (d) and open field (e) at the temperate forest.
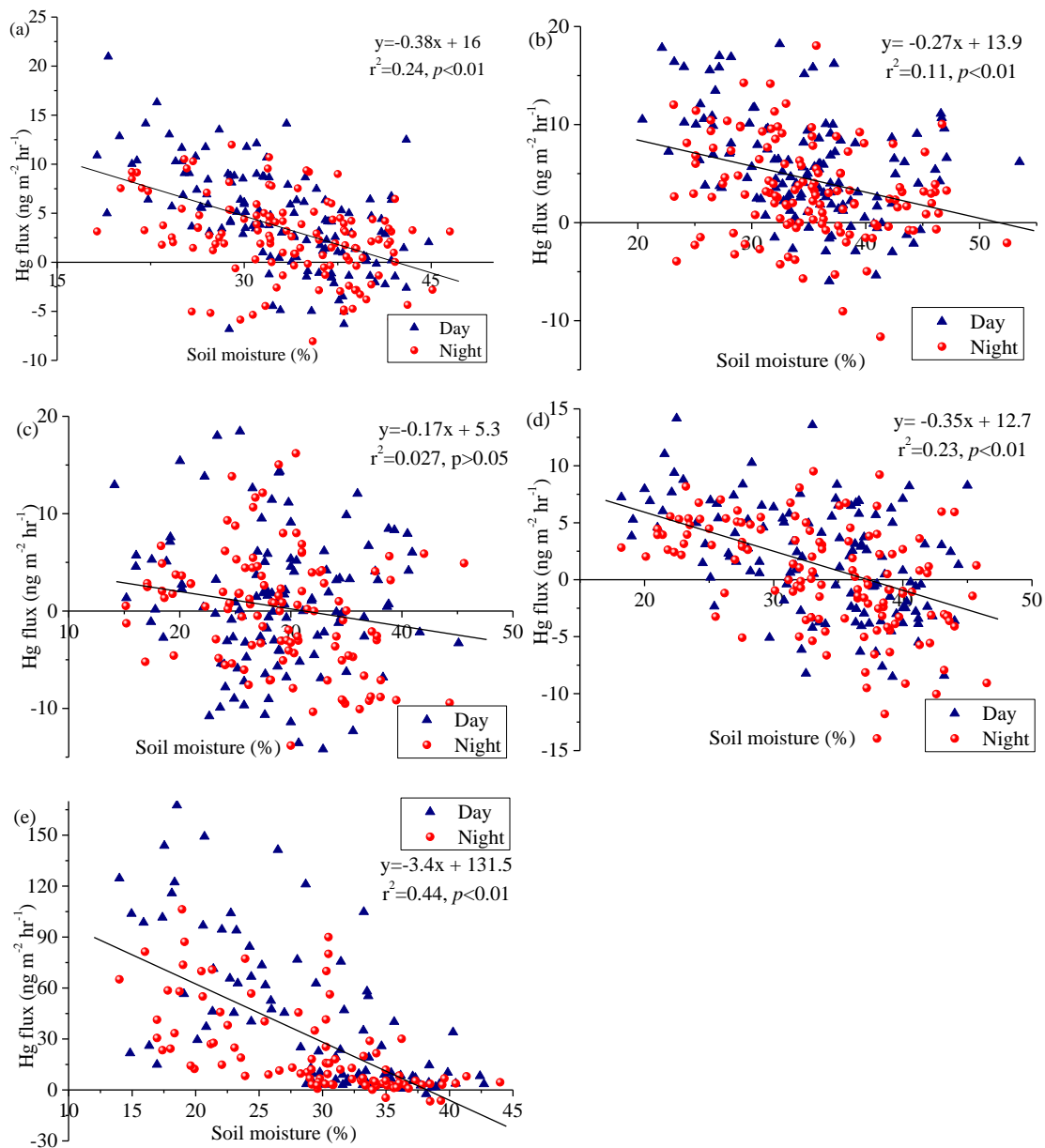
1285

1286

1287

1288

Fig. S9. Correlations between soil moisture and air-surface Hg fluxes measured during daytime and
night at the Chinese pine forest (a), larch forest (b), wetland (c), mixed broad-leaved forest (d) and
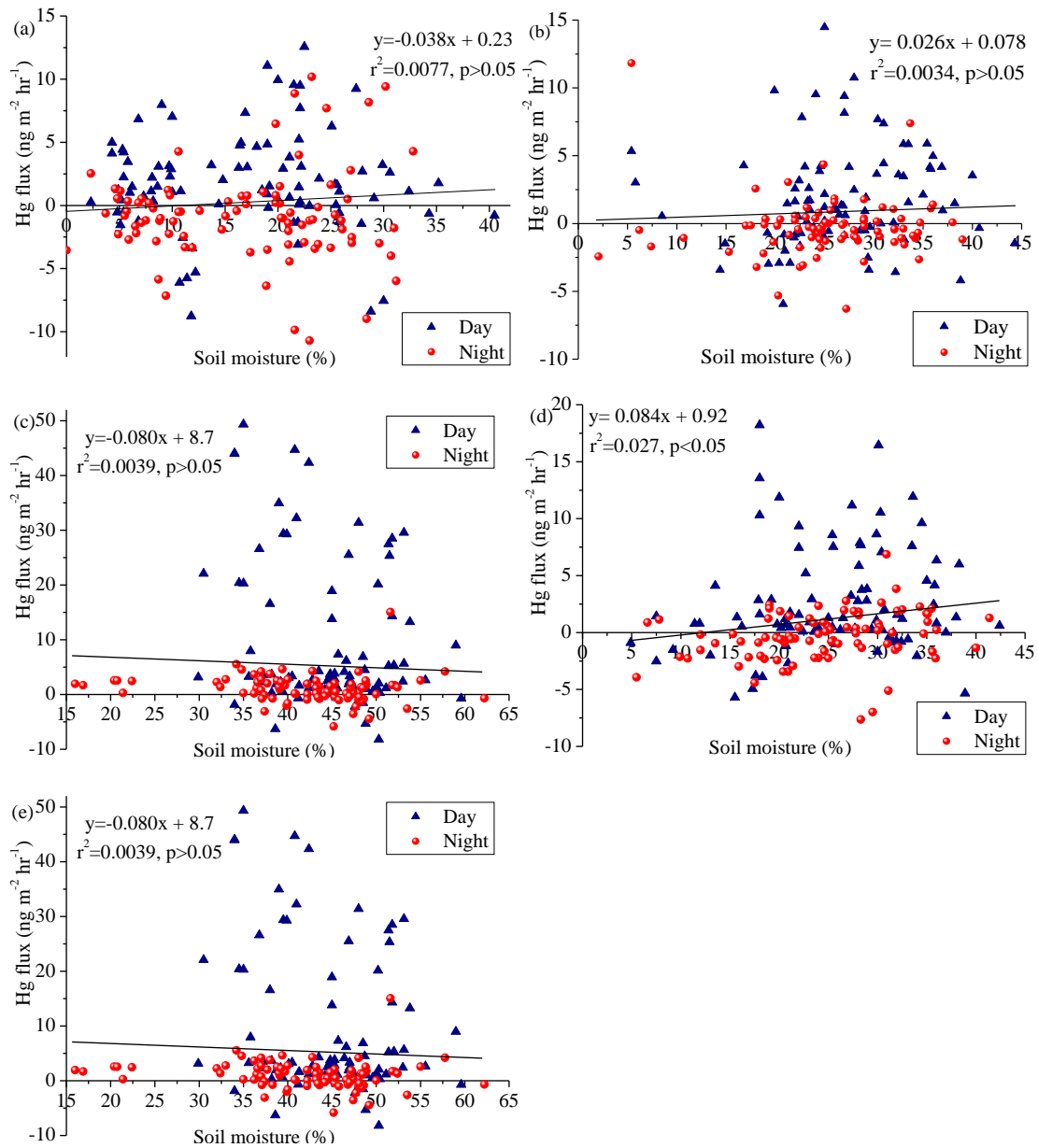open field (e) at the subtropical forest.

1293

1294

1295

Fig. S10. Correlations between soil moisture and air-surface Hg fluxes measured during daytime and night at the Chinese pine forest (a), larch forest (b), wetland (c), mixed broad-leaved forest (d) and open field (e) at the temperate forest.
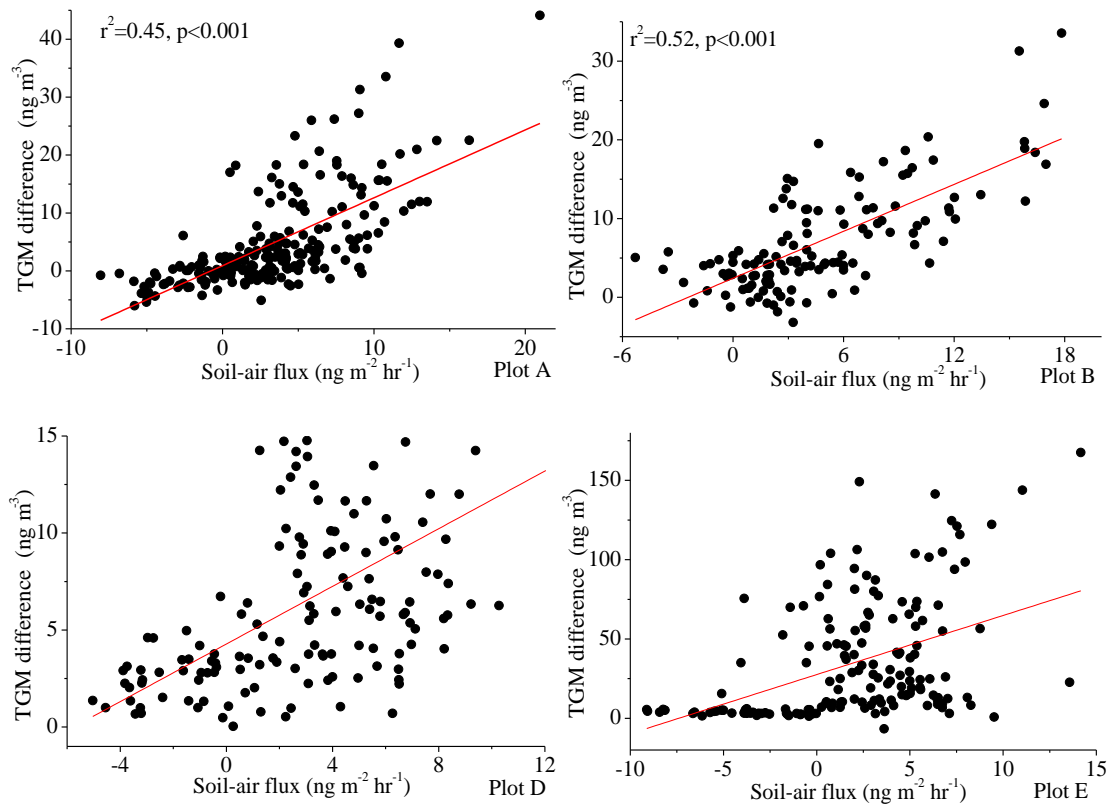
1296
1297
1298

1299

1300

1301

Fig. S11. Correlations between the gradient of Hg(0) concentrations between surface soil pore (at 3 cm) and atmospheric values and soil-air Hg(0) flux at four plots at the subtropical forest.
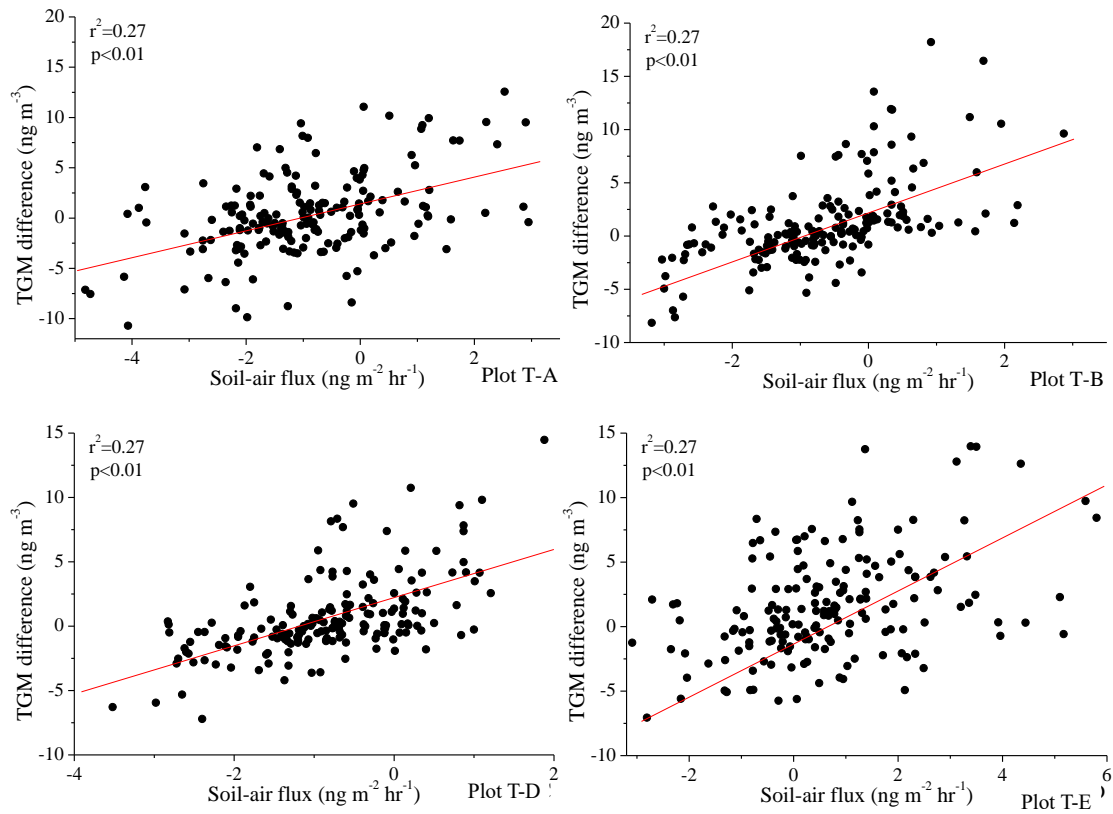
1302

1303

1304

1305

1306

Fig. S12. Correlations between the gradient of Hg(0) concentrations between surface soil pore (at 3 cm) and atmospheric values and soil-air Hg(0) flux at the four plots at the temperate forest.

1307

1308

1309

References:

Zhou, H., Ma, K., and Fu, B.: Analysis of the impacts of human activities on landscape patterns in dangling mountain area of Beijing, J Nat Resour, 14, 117-122, 1999.

Zhou, J., Feng, X., Liu, H., Zhang, H., Fu, X., Bao, Z., Wang, X., and Zhang, Y.: Examination of total mercury inputs by precipitation and litterfall in a remote upland forest of Southwestern China, Atmospheric Environment, 81, 364-372, 10.1016/j.atmosenv.2013.09.010, 2013.

Zhou, J., Wang, Z., Zhang, X., and Chen, J.: Distribution and elevated soil pools of mercury in an acidic subtropical forest of southwestern China, Environmental Pollution, 202, 187-195, 10.1016/j.envpol.2015.03.021, 2015.

Zhou, J., Wang, Z., Sun, T., Zhang, H., and Zhang, X.: Mercury in terrestrial forested systems with highly elevated mercury deposition in southwestern China: The risk to insects and potential release from wildfires, Environmental Pollution, 212, 188-196, 10.1016/j.envpol.2016.01.003, 2016.

Zhou, J., Wang, Z., Zhang, X., and Gao, Y.: Mercury concentrations and pools in four adjacent coniferous and deciduous upland forests in Beijing, China, Journal of Geophysical Research: Biogeosciences, 122, 1260-1274, 2017.

Zhu, J., Mulder, J., Solheimslid, S. O., and Dörsch, P.: Functional traits of denitrification in a subtropical forest catchment in China with high atmogenic N deposition, Soil Biology and Biochemistry, 57, 577-586, https://doi.org/10.1016/j.soilbio.2012.09.017, 2013.